Cell Reports

Article

# Disrupting mitochondrial dynamics attenuates ferroptosis and chemotoxicity via upregulating NRF2-mediated FSP1 expression

## Graphical abstract

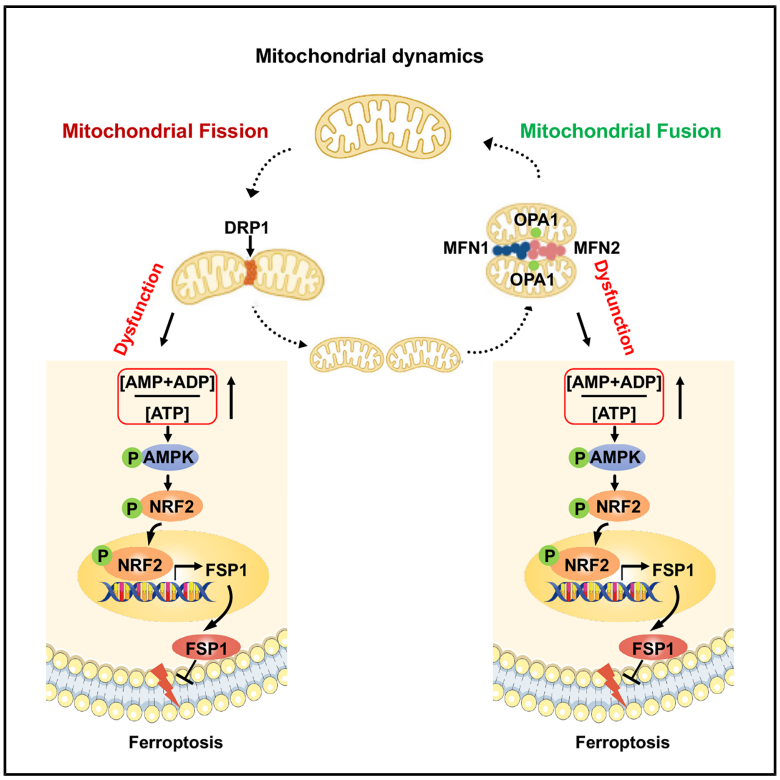


## Highlights

- Disruption of mitochondrial dynamics inhibits ferroptosis
- Defects in mitochondrial dynamics impair ATP generation and activate AMPK
- AMPK phosphorylates and promotes NRF2 nuclear relocation to drive FSP1 expression
- Mitochondrial fusion promoter M1 mitigates doxorubicin-induced chemotoxicity

## Authors

Shuang Ma, Jianhua Qin, Yao Zhang, ..., Yang Xiao, Wei Zhang, Minghui Gao

## Correspondence

weizhang19823@gmail.com (W.Z.), gaominghui@hit.edu.cn (M.G.)

## In brief

Ma et al. discovered that the disruption of mitochondrial dynamics impairs ATP generation and activates AMPK, which phosphorylates NRF2, facilitating its translocation to the nucleus. Within the nucleus, NRF2 drives FSP1 expression and confers resistance to ferroptosis. They also identified that mitochondrial fusion promoter M1 mitigates doxorubicin-induced chemotoxicity.

Ma et al., 2025, Cell Reports *44*, 116234
September 23, 2025 
https://doi.org/10.1016/j.celrep.2025.116234

CellPress

Cell Reports

CellPress
OPEN ACCESS

Article

# Disrupting mitochondrial dynamics attenuates ferroptosis and chemotoxicity via upregulating NRF2-mediated FSP1 expression

Shuang Ma,[1,3] Jianhua Qin,[1,3] Yao Zhang,[1] Jing Luan,[1] Na Sun,[1] Guoyuan Hou,[1] Jiyuan He,[1] Yang Xiao,[1] Wei Zhang,[2,*] and Minghui Gao[1,4,*]

[1]The HIT Center for Life Sciences, School of Life Science and Technology, Harbin Institute of Technology, Harbin 150080, China
[2]Department of Microbiology and Immunology, Weill Cornell Medicine, 1300 York Avenue, New York, NY 10065, USA
[3]These authors contributed equally
[4]Lead contact
*Correspondence: weizhang19823@gmail.com (W.Z.), gaominghui@hit.edu.cn (M.G.)
https://doi.org/10.1016/j.celrep.2025.116234

## SUMMARY

Ferroptosis is a regulated necrosis driven by iron-dependent lipid peroxidation. Mitochondria play vital roles in ferroptosis. Mitochondrial dynamics is critical for the health of mitochondria and cells. But how this process regulates ferroptosis is not fully understood. Here, we found that mitochondrial fission is induced during ferroptosis. Disruption of mitochondrial dynamics by impeding the expression of the central players of mitochondrial dynamics control, dynamin-related protein 1 (DRP1) and Mitofusion1/2, or modifying the expression of optic atrophy 1 (OPA1) inhibits ferroptosis. Mechanistically, a defect in mitochondrial dynamics homeostasis increases the ratio of [AMP+ADP]/[ATP], thus activating AMP-activated protein kinase (AMPK), which further phosphorylates nuclear factor erythroid 2-related factor 2 (NRF2) and promotes NRF2 nuclear translocation. Subsequently, NRF2 triggers ferroptosis suppressor 1 (FSP1) upregulation, which renders the cells resistant to ferroptosis. Importantly, mitochondrial fusion promoter M1 can mitigate the chemotoxicity induced by doxorubicin without compromising its anti-cancer efficacy. Collectively, the results of this study demonstrate the crucial role of mitochondrial dynamics in ferroptosis and indicate a potential therapeutic protective approach for chemotoxicity.

## INTRODUCTION

Ferroptosis has emerged as an iron-dependent form of regulated cell death modality highly relevant to human disease.[1–4] Ferroptosis was initially discovered as an iron-dependent non-apoptotic cell death induced by a series of synthetic small-molecule compounds, such as erastin and RSL3 (namely, ferroptosis-inducing agents [FINs]). Execution of ferroptosis requires the accumulation of phospholipid peroxidation. Erastin activates ferroptosis by inhibiting the activity of system $Xc^-$, a cystine-glutamate antiporter, resulting in the depletion of cellular cysteine and glutathione (GSH), thus breaking cellular redox homeostasis.[5] Inactivation of glutathione peroxidase 4 (GPX4), an enzyme required to remove the toxic oxidized phospholipid, can induce ferroptosis even in the presence of cellular cysteine and GSH.[6–8] The ferroptosis suppressor 1 (FSP1) replenishes a reduced form of ubiquinone, called ubiquinol, that protects against ferroptosis by combating lipid peroxidation.[9,10]

Since the term "ferroptosis" was coined, various investigations have established the involvement of ferroptosis in multiple human diseases. For example, ferroptosis is involved in ischemia-induced organ injury, including brain damage, heart diseases, and acute renal failure.[7,11–14] Marked protection by ferroptosis inhibitors was also demonstrated in animal models of neurodegenerative diseases.[15,16] Ferroptosis has been shown to contribute to the tumor-suppressive function of p53,[17–20] BAP1,[21,22] and fumarase.[23] Numerous studies have shown that the activation of certain oncogenes or the inactivation of certain tumor suppressors sensitizes cancer cells to ferroptosis.[24–28] Ferroptosis was also shown to be crucial for cancer immunotherapy[29] and radiotherapy.[30] These findings suggest that targeting ferroptosis, either inducing or inhibiting it, might be a potential therapeutic approach in treating related diseases.

Cellular metabolism, which includes lipid metabolism and amino acid metabolism (particularly that involving cysteine and glutamine), is essential for ferroptosis.[2,3] Autophagy promotes ferroptosis by degrading ferritin and increasing cellular labile iron.[31,32] The canonical metabolic activity of mitochondria, including both the tricarboxylic acid (TCA) cycle and mitochondrial electron transport chain (ETC) activity, are required for the generation of enough phospholipid peroxides to initiate ferroptosis.[23] Glucose, the most abundant nutrient, is required for ferroptosis. Upon glucose starvation, AMP-activated protein kinase (AMPK), the cellular energy sensor, is activated and negatively regulates ferroptosis.[27,33] Mitochondrial fission and fusion have been recognized as crucial processes in the normal function of

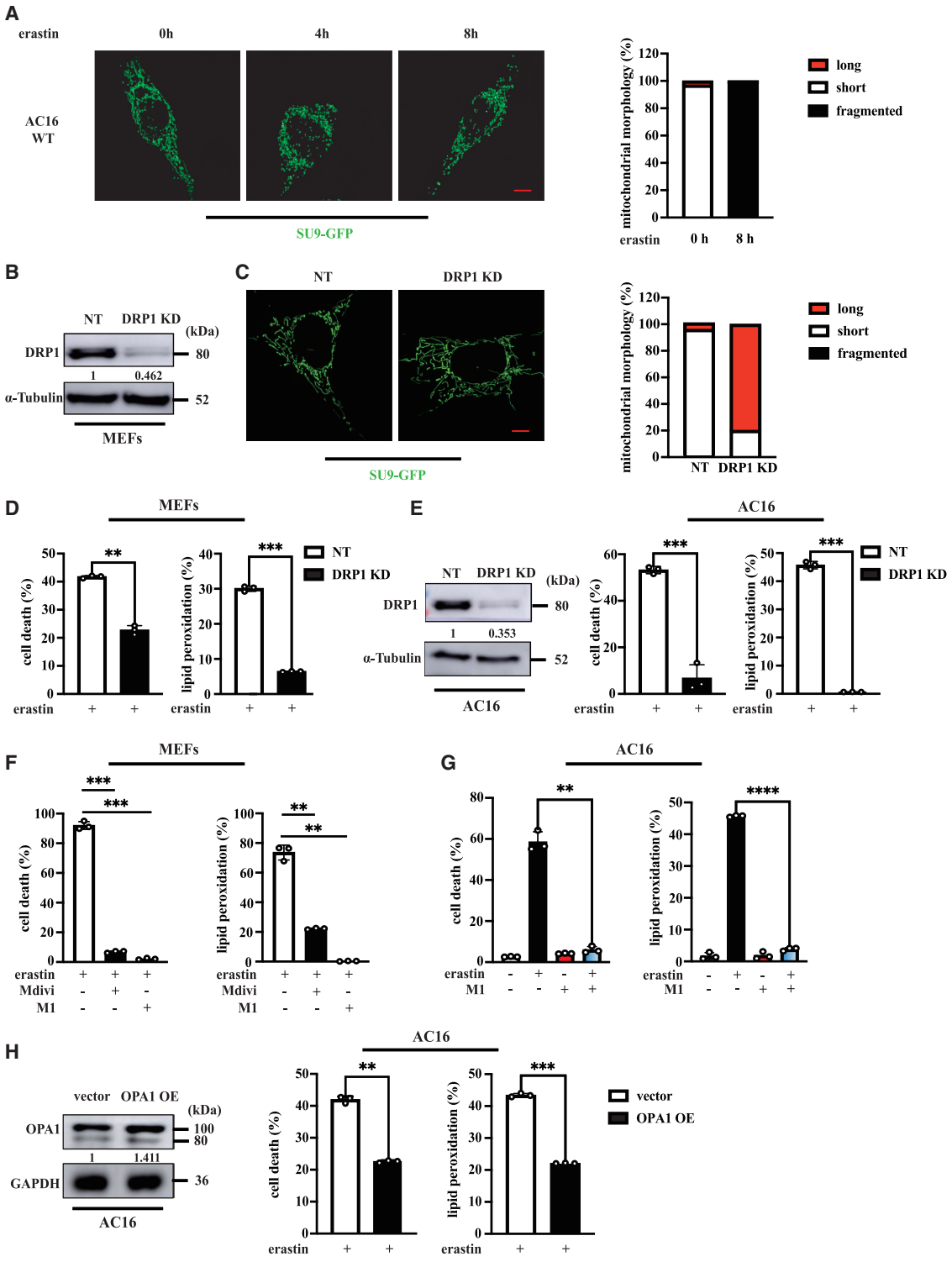


**Figure 1. Promoting mitochondrial fusion blocks ferroptosis**

(A) Fragmentation of mitochondria is associated with ferroptosis in AC16 cells. SU9-GFP AC16 cells were treated with erastin (20 μM) as indicated. SU9-GFP-labeled mitochondria were imaged using a confocal laser scanning microscope (scale bars in the images of all figures represent 10 μM). Quantification of mitochondria with different morphology (fragmented, short, or long). "Short" represents cells with a majority of mitochondria shorter than 10 μm, "long" represents cells with a majority of mitochondria longer than 10 μm, and "fragmented" represents cells with a majority of granular mitochondria. At least 100 cells were counted for each sample.

*(legend continued on next page)*

mitochondria and cells.[34] A dramatic fragmentation of mitochondria during ferroptosis was observed by several groups.[35] However, less is known about the role of mitochondrial fragmentation in ferroptosis.

This study elucidates the critical role of mitochondrial dynamics homeostasis in ferroptosis. We demonstrate that genetic depletion or pharmacological inhibition of dynamin-related protein 1 (DRP1) markedly suppresses ferroptotic cell death. In parallel, the promotion of mitochondrial fusion through the overexpression of optic atrophy 1 (OPA1) effectively blocks ferroptosis. Interestingly, enhancing mitochondrial fission by genetic knockdown (KD) of Mitofusion1/2 or OPA1 also significantly mitigates ferroptosis, underscoring the importance of balanced mitochondrial dynamics for this process. Mechanistically, disruption of mitochondrial dynamics equilibrium leads to an increased cellular [AMP+ADP]/[ATP] ratio, thereby activating AMPK. This activation results in the phosphorylation of nuclear factor erythroid 2-related factor 2 (NRF2), promoting its nuclear accumulation. Subsequently, NRF2 upregulates the expression of FSP1, conferring resistance to ferroptosis. Furthermore, we provide evidence suggesting that the modulation of mitochondrial dynamics represents a promising therapeutic strategy for mitigating doxorubicin (Dox)-induced chemotoxicity. Collectively, our findings highlight the pivotal role of mitochondrial dynamics homeostasis in the regulation of ferroptosis.

## RESULTS

### Promoting mitochondrial fusion blocks ferroptosis

Mitochondria are highly dynamic organelles that undergo constant cycles of fusion and fission.[36] Dramatic fragmentation of interconnected reticular networks of mitochondria is associated with erastin-induced ferroptosis[35,37] (Figure 1A). This phenomenon prompted us to test if inhibiting mitochondrial fragmentation or fission could prevent ferroptosis. DRP1, a GTPase, is required for mitochondrial fission in mammals.[36] As shown in Figures 1B and 1C, KD of DRP1 in mouse embryonic fibroblasts (MEFs) using a short hairpin RNA (shRNA) sequence resulted in a highly elongated mitochondrial network, as expected.[38] We treated the cells with the ferroptosis inducer erastin and found that the sensitivity of DRP1-KD MEFs to lipid reactive oxygen species (ROS) accumulation and ferroptosis was significantly decreased compared to that of control cells (non-targeting, NT) (Figure 1D). Similarly, KD of DRP1 also protected human cardiomyocyte AC16 cells from ferroptosis and lipid peroxidation (Figure 1E). Consistently, pharmacological inhibition of DRP1 by its small-molecule inhibitor Mdivi-1 or promoting mitochondrial fusion with small molecular MFP M1 (mitochondrial fusion promoter M1) can inhibit lipid peroxidation and ferroptosis (Figures 1F and 1G) in both MEFs and AC16 cells. As expected, mitochondrial fragmentation induced by erastin was completely blocked by knocking down DRP1 (Figure S1A) or treating with MFP M1 (Figure S1B) in AC16 cells. OPA1 is an essential GTPase responsible for the fusion of the mitochondrial inner membrane.[39] We found that overexpression of OPA1 could also suppress ferroptosis sensitivity (Figure 1H). These data suggest that the promotion of mitochondrial fusion suppresses ferroptosis. RSL3 or ML162 induces ferroptosis by directly inhibiting GPX4. We found that promoting mitochondrial fusion by knocking down DRP1 or overexpressing (OE) OPA1 could not block RSL3- or ML162-treatment-induced ferroptosis (Figures S1C and S1D), which is consistent with our previous study that mitochondria are required for cysteine-depletion-induced ferroptosis but not for GPX4-depletion-induced ferroptosis.[23]

### Promoting mitochondrial fission alleviates ferroptosis

Given the crucial negative role of the mitochondrial fusion process in ferroptosis, we expected that promoting mitochondrial fission with inactivation of mitofusin 1 (MFN1) or mitofusin 2 (MFN2), the master regulators of mitochondrial fusion,[40] would sensitize cells to ferroptosis. To test this idea, we generated MFN1-knockout (MFN1-KO) MEFs with CRISPR-Cas9 technology and determined their sensitivity to ferroptosis. As shown in Figures 2A and 2B, depletion of MFN1 resulted in mitochondrial fragmentation, as reported previously.[41] We then assessed the sensitivity to ferroptosis in MFN1-KO cells. To our surprise, KO of MFN1 confers MEF resistance to lipid peroxidation and ferroptosis induced by erastin (Figure 2C). However, KO of MFN1 cannot suppress RSL3- (Figure S2A) or ML162- (Figure S2B) induced ferroptosis. Similarly, KD of MFN2 in MEFs significantly conferred cells' resistance to lipid peroxidation and ferroptosis induced by erastin compared to that of control cells (Figure 2D). Consistently, knocking down OPA1 in AC16 cells ameliorates ferroptosis sensitivity (Figure 2E), which was also observed recently by another group.[42] The above data suggest that the enhancement of mitochondrial fission blocks ferroptosis.

(B–E) KD of DRP1 blocks lipid ROS accumulation and ferroptosis.
(B)Western blot analysis of DRP1 expression in control MEFs and DRP1-KD MEFs.
(C) SU9-GFP-labeled mitochondria in control MEFs or DRP1-KD MEFs were imaged using a confocal laser scanning microscope.
(D) Control MEFs and DRP1-KD MEFs treated with erastin (10 μM) for 8 h for cell death measurement or 6 h for lipid ROS measurement. Cell death was measured with phosphatidylinositol (PI) staining coupled with flow cytometry. The accumulation of lipid ROS was assessed by BODIPY C11 staining coupled with flow cytometry analysis.
(E) Western blot analysis of DRP1 expression in NT AC16 cells and DRP1-KD AC16 cells. The cells were treated with erastin (20 μM) for 16 h for cell death measurement or 12 h for lipid ROS measurement.
(F and G) Mdivi-1 or MPF M1 inhibits lipid peroxidation and ferroptosis.
(F) MEFs were treated with erastin (10 μM), Mdivi (10 μM), or MFP M1 (10 μM) for 8 h for cell death measurement or 6 h for lipid ROS measurement.
(G) AC16 cells were treated with erastin (20 μM) or MFP M1 (20 μM) for 16 h for cell death measurement or 12 h for lipid ROS measurement.
(H) Western blot analysis of OPA1 expression in vector control and OPA1-OE AC16 cells. The cells were treated with erastin (20 μM) for 16 h for cell death measurement or 12 h for lipid ROS measurement.
All quantitative data are presented as mean ± SD from three independent experiments, and $p$ values were calculated with an unpaired t test (*$p < 0.05$, **$p < 0.01$, ***$p < 0.001$, and ****$p < 0.0001$).

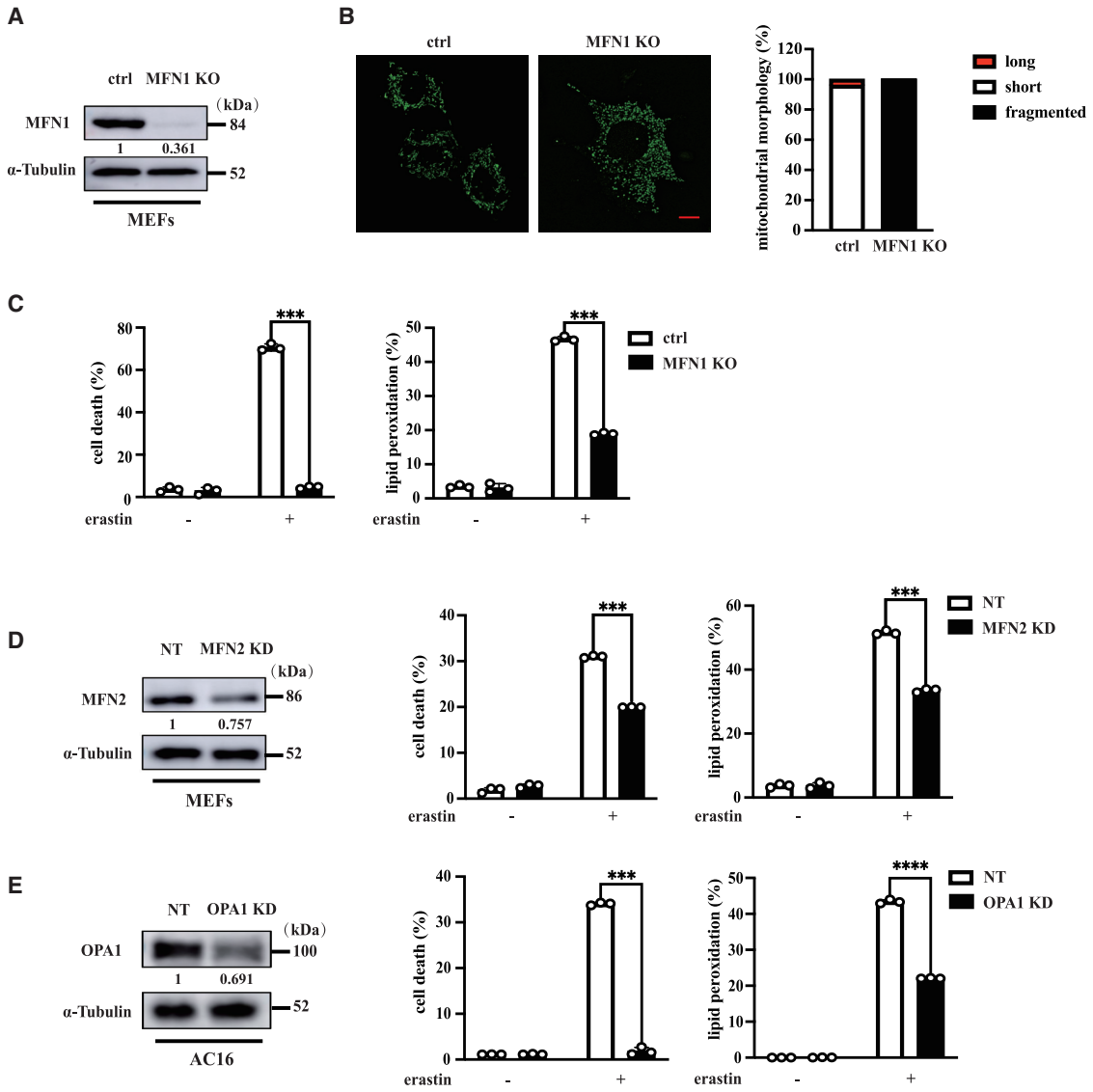


**Figure 2. Promoting mitochondrial fission alleviates ferroptosis**

(A and B) Depletion of MFN1 resulted in mitochondrial fragmentation.

(A) Western blot analysis of MFN1 expression in control MEFs and MFN1-KO MEFs.

(B) SU9-GFP-labeled mitochondria in control MEFs or MFN1-KO MEFs were imaged using a confocal laser scanning microscope.

(C) KO of MFN1 confers MEF resistance to lipid peroxidation and ferroptosis. Control MEFs and MFN1-KO MEFs were treated with erastin (10 μM) for 8 h for cell death measurement or 6 h for lipid ROS measurement.

(D) KD of MFN2 confers MEF resistance to lipid peroxidation and ferroptosis. Western blot analysis of MFN2 in NT MEFs and MFN2-KD MEFs. NT MEFs and MFN2-KD MEFs were treated with erastin (10 μM) for 8 h for cell death measurement or 6 h for lipid ROS measurement.

(E) KD of OPA1 confers AC16 cells resistance to lipid peroxidation and ferroptosis. Western blot analysis of OPA1 in NT and OPA1-KD AC16 cells. NT and OPA1-KD AC16 cells were treated with erastin (20 μM) for 16 h for cell death measurement or 12 h for lipid ROS measurement.

All quantitative data are presented as mean ± SD from three independent experiments, and $p$ values were calculated with an unpaired t test (*$p < 0.05$, **$p < 0.01$, ***$p < 0.001$, and ****$p < 0.0001$).

## Defects in mitochondrial dynamics protect cells from ferroptosis by upregulating FSP1

We next tried to determine the molecular mechanism by which disrupting mitochondrial dynamics attenuates ferroptosis. We hypothesized that one or more negative regulators of ferroptosis may be upregulated after mitochondrial dynamics machine proteins were depleted. We compared the protein levels of three well-studied negative regulators of ferroptosis, SLC7A11,[35] GPX4,[6] and FSP1,[9,10] between control and DRP1-KD cells and found that the expression of FSP1 dramatically increased in DRP1-KD AC16 cells (Figure 3A). Consistently, FSP1 was upregulated by MFP M1 treatment (Figure 3B) or overexpression of

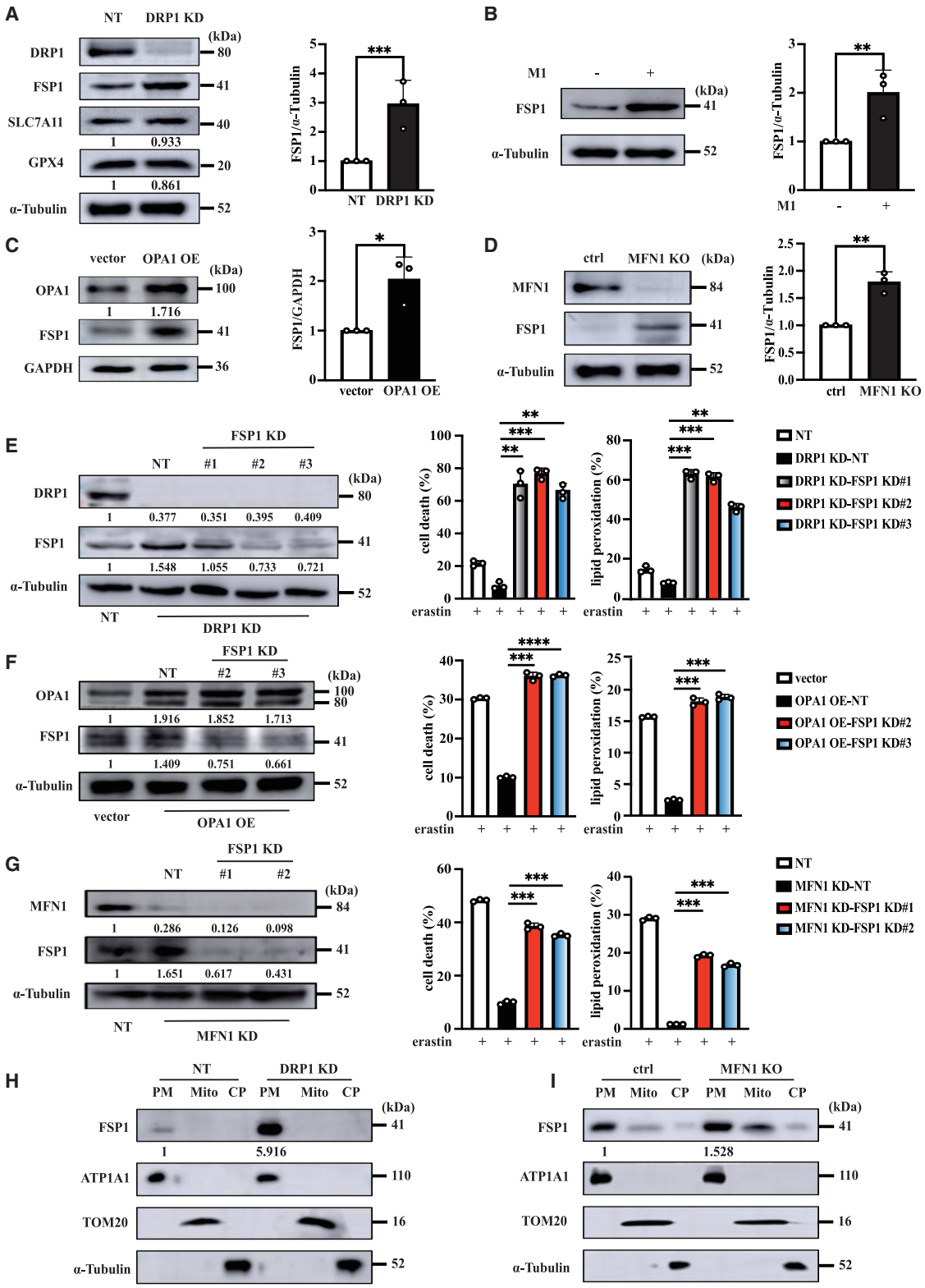


**Figure 3. Defects in mitochondrial dynamics protect cells from ferroptosis by upregulating FSP1**

(A) The expression of FSP1 is increased in DRP1-KD cells. Left: western blot analyzing the expression of indicated proteins in NT AC16 cells and DRP1-KD AC16 cells. Right: quantity analysis of expression of FSP1.

*(legend continued on next page)*

OPA1 in AC16 cells (Figure 3C). Similarly, the upregulation of the protein level of FSP1 was also observed in MFN1-KO MEFs (Figure 3D). We further detected the mRNA level of FSP1 and found that FSP1 was transcriptionally upregulated in DRP1-KD cells, OPA1-OE cells, MFN1-KO cells, and MFP M1-treated cells (Figures S3A–S3D). More importantly, KD of FSP1 in DRP1-KD AC16 cells (Figure 3E), OPA1-OE AC16 cells (Figure 3F), or MFN1-KD MEFs (Figure 3G) cells significantly rescued the sensitivity to lipid peroxidation and ferroptosis. Remarkably, we found that increased FSP1 was mainly accumulated on the plasma membrane upon depletion of DRP1 (Figure 3H) or MFN1 (Figure 3I), consistent with previous reports that cell-membrane-localized FSP1 suppresses ferroptosis.[9,10]

## NRF2 is required for the upregulation of FSP1 induced by defects of mitochondrial dynamics homeostasis

It was reported that the accumulation of lipid peroxides activates the NRF2-mediated antioxidant defense system to protect against ferroptotic cell death.[43] FSP1-ubiquinol is a vital antioxidant system that prevents cell death by ferroptosis.[9,10] We thus tested whether defects in mitochondrial dynamics homeostasis-induced upregulation of FSP1 and ferroptosis resistance depend on NRF2. As shown in Figures 4A–4C, treatment with ML385, a NRF2-specific small-molecular inhibitor, can dramatically restore the sensitivity to the lipid peroxidation and ferroptosis in DRP1-KD cells (Figure 4A), OPA1-OE cells (Figure 4B), or MFN1-KO cells (Figure 4C). The upregulation of FSP1 in DRP1-KD cells, OPA1-OE cells, or MFN1-KO cells was also significantly blocked by ML385 treatment at both the RNA level (Figures S4A–S4C) and the protein level (Figures 4D–4F). To rule out the off-target effect of NRF2 inhibitors, we generated NRF2-KD cells using two independent shRNAs in cells with different genetic backgrounds and tested their ferroptosis sensitivity and FSP1 levels in these cells. Consistent with the effect of NRF2 inhibitor ML385, knocking down NRF2 in DRP1-KD cells (Figure 4G), OPA1-OE cells (Figure 4H), or MFN1-KD MEFs (Figure 4I) restored the sensitivity to lipid peroxidation and ferroptosis. The upregulation of FSP1 in DRP1-KD cells (Figure 4J), OPA1-OE cells (Figure 4K), or MFN1-KD cells (Figure 4L) was also blocked by knocking down NRF2 at both the protein level and the RNA level (Figures S4D–S4F).

KEAP1 negatively regulates NRF2 stability. We further analyzed dysfunctional mitochondrial dynamics-induced expression of FSP1 in A549 cells, a KEAP1-mutant cancer cell. As shown in Figure S4G, disruption of mitochondrial dynamics upregulates FSP1 expression in A549 cells, suggesting that KEAP1 is not required for the upregulation of FSP1 induced by the disruption of mitochondrial dynamics.

## Defects in mitochondrial dynamics homeostasis stabilize NRF2 and promote NRF2 accumulation in the nucleus, and NRF2 triggers the upregulation of FSP1

We then addressed how mitochondrial hemostasis regulates NRF2. We first observed that KD of DRP1, overexpression of OPA1, or depletion of MFN1 could increase the protein level of NRF2 in both AC16 stable cells (Figures 5A–5C, input) and 293T transient expression conditions (Figures 5D–5F, input). We further demonstrated that disruption of mitochondrial dynamics homeostasis induces NRF2 upregulation by inhibiting its ubiquitination in both AC16 stable cells (Figures 5A–5C, immunoprecipitation [IP]) and 293T transient expression conditions (Figures 5D–5F, IP).

NRF2 is a transcriptional factor, so we hypothesized that the subcellular localization of NRF2 may also be changed in the cells with defects in mitochondrial dynamics homeostasis. By cellular fraction assay, we found that NRF2 was accumulated in the nucleus in DRP1-KD cells (Figure 5G), OPA1-OE cells (Figure 5H), or MFN1-KO cells (Figure 5I). Similarly, defects in mitochondrial dynamics homeostasis promote NRF2 nuclear accumulation in A549 cells (Figures S5A–S5D). We found there are two putative NRF2 binding sites on the promoter region of FSP1, according to the JASPAR transcription factor binding profile database.[44] The first binding site is at −1,480, and the second binding site is at −979 (Figure 5J). We then confirmed that NRF2 can bind at −979 sites and that FSP1 is a target of NRF2 by chromatin IP assay (Figure 5K). Importantly, both DRP1 KD (Figure 5L) and mitochondria fusion promoter M1 treatment (Figure 5M)

(B) Treatment with MFP M1 increases the expression of FSP1 in AC16 cells. Left: western blot analysis of FSP1 expression in wild-type AC16 cells treated with MPF M1 (20 μM) for 12 h. Right: quantity analysis of FSP1 expression.
(C) The expression of FSP1 increased in OPA1-OE AC16 cells. Left: western blot analysis of FSP1 expression in vector control and OPA1-OE AC16 cells. Right: quantity analysis of expression of FSP1.
(D) The expression of FSP1 is increased in MFN1-KO cells. Left: western blot analysis of FSP1 expression in control MEFs and MFN1-KO MEFs. Right: quantity analysis of FSP1 expression in the western blot.
(E) KD of FSP1 in DRP1-KD cells restores the sensitivity to lipid peroxidation and ferroptosis. Left: western blot analysis of FSP1 expression in indicated AC16 cells. Right: AC16 cells as indicated were treated with erastin (20 μM) for 16 h for cell death measurement or 12 h for lipid ROS measurement.
(F) KD of FSP1 in OPA1-OE cells restores the sensitivity to ferroptosis. Left: western blot analysis of the expression of FSP1 in indicated AC16 cells. Right: indicated AC16 cells were treated with erastin (20 μM) for 16 h for cell death measurement or 12 h for lipid ROS measurement.
(G) KD of FSP1 in MFN1-KD MEFs restores the sensitivity to ferroptosis. Left: western blot analysis of the expression of FSP1 in indicated MEFs. Right: MEFs as indicated were treated with erastin (10 μM) for 8 h for cell death measurement or 6 h for lipid ROS measurement.
(H and I) Increased plasma membrane accumulation of FSP1 in DRP1-KD cells and MFN1-KO cells.
(H) Western blot analysis of ATP1A1, FSP1, α-tubulin, and TOM20 in indicated AC16 cells. ATP1A1: the biomarker of plasma membrane (PM), α-Tubulin: the biomarker of cytoplasm (CP), and TOM20: the biomarker of mitochondria (Mito).
(I) Western blot analysis of ATP1A1, FSP1, α-Tubulin, and TOM20 in indicated MEFs. ATP1A1: the biomarker of PM, α-Tubulin: the biomarker of CP, and TOM20: the biomarker of Mito.
All quantitative data are presented as mean ± SD from three independent experiments, and $p$ values were calculated with an unpaired t test (*$p < 0.05$, **$p < 0.01$, ***$p < 0.001$, and ****$p < 0.0001$).

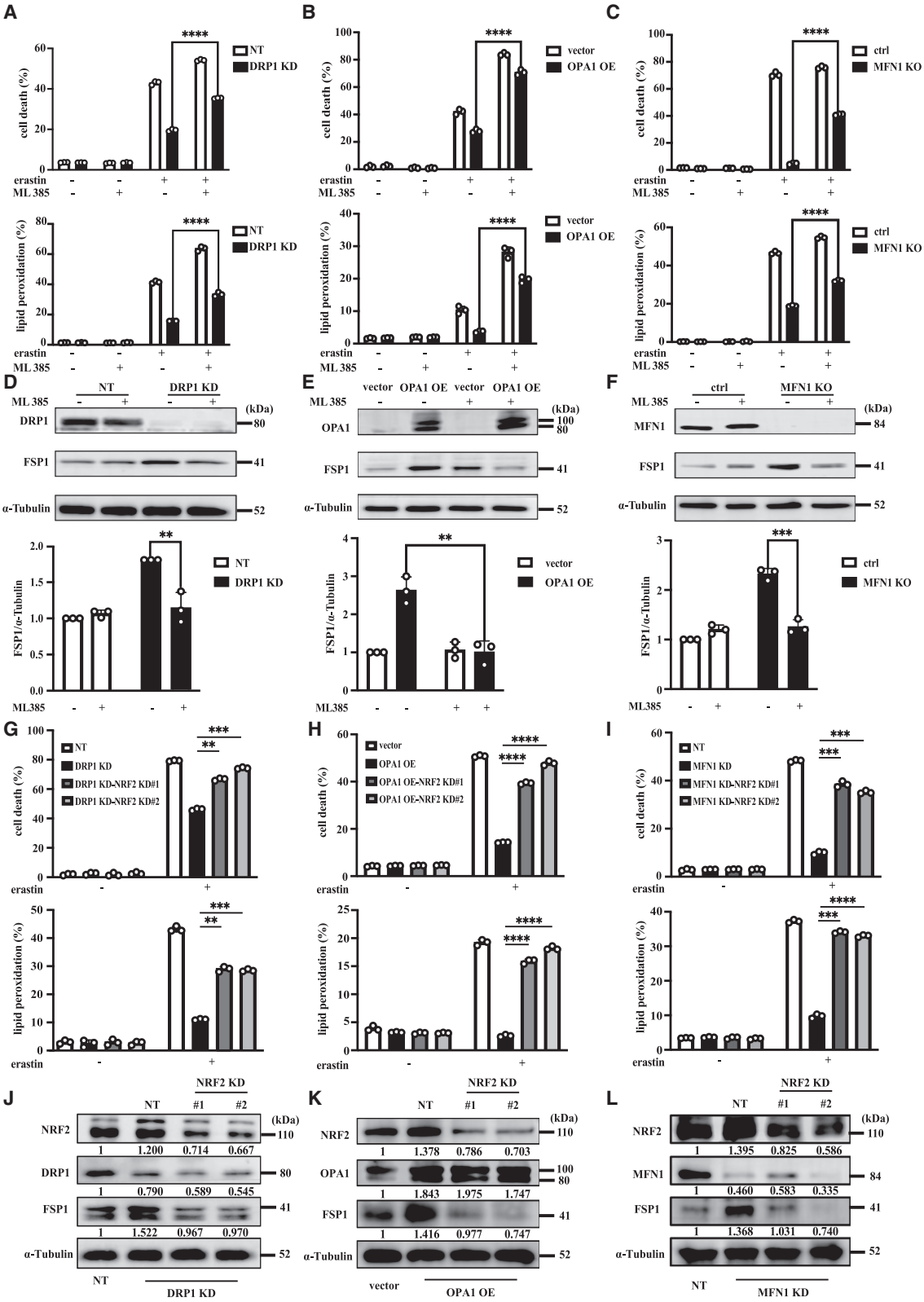


*(legend on next page)*

could further promote the binding of NRF2 to the promoter region of the FSP1 gene.

### Phosphorylation of NRF2 by AMPK is required for NRF2 nuclear accumulation, FSP1 upregulation, and ferroptosis resistance in mitochondrial dynamics-defected cells

How do defects of mitochondrial dynamics promote NRF2 nuclear accumulation? Mitochondrial dynamics homeostasis is crucial for the function of mitochondria. Defects in mitochondrial dynamics homeostasis may impair mitochondrial energy production. As shown in Figures 6A and S6A, the ATP level is significantly lower in mitochondrial dynamics-defected cells, and the ratio of [AMP+ADP]/[ATP] is significantly higher in mitochondrial dynamics-defected cells. The decrease in ATP is due to the downregulated protein level of ETC components (including complexes I, II, III, IV, and V) in cells with disrupted mitochondrial dynamics (Figure S6B). A high ratio of [AMP+ADP]/[ATP] could activate the master cellular energy sensor AMPK. We found that the phosphorylation of $AMPK^{T172}$ and its downstream substrate Acetyl-CoA carboxylase (ACC) significantly increases in the cells with depletion of DPR1 or MFN1, or overexpression of OPA1, compared to control cells (Figure 6B). We also measured the total ROS with H2DCFDA dye staining and mitochondrial ROS with MitoSOX dye staining. As shown in Figures S6C and S6D, both total ROS and mitochondrial ROS are significantly lower in the cells with disrupted mitochondrial dynamics, suggesting that the activation of AMPK is not due to high levels of ROS stress in these cells (Figures S6C and S6D). AMPK could phosphorylate NRF2 at Ser550 and promote NRF2 nuclear translocation.[45] Since the commercial antibody against NRF2 Ser550 is not available, NRF2 was immunoprecipitated and then blotted with the antibody of the phospho-AMPK substrate motif. We found that the phosphorylation of NRF2 significantly increases in the cells with depletion of DPR1, overexpression of OPA1, or KO of MFN1 compared to control cells (Figures 6C–6E). We observed that the interaction between NRF2 and AMPK is upregulated in mitochondrial dynamics-defected cells (Figures 6C–6E). Interestingly, compared to wild-type NRF2, the phospho-defective mutant NRF2 is less stable (Figure S6E) and more polyubiquitinated (Figure S6F), and the interaction with KEAP1 is much stronger (Figure S6F). Furthermore, depletion of AMPK could block the nuclear translocation of NRF2 (Figures 6F–6H) and the upregulation of FSP1 (Figures 6I–6K) in mitochondrial dynamics-defected cells. More importantly, depletion of AMPK could significantly restore the ferroptosis sensitivity of the cells with defective mitochondrial dynamics (Figures 6L–6N).

### MFP M1 protects against Dox-induced chemotoxicity without compromising its chemotherapeutic efficacy

Dox is an effective chemotherapeutic agent for diverse cancer treatments. However, the clinical application of Dox is severely limited by its chemotoxicity, especially its cardiotoxicity. Ferroptosis was reported as a target for Dox-induced chemotoxicity.[46] We thus determined whether manipulating mitochondrial dynamics homeostasis can alleviate Dox-induced chemotoxicity. As shown in Figure 7A, MFP M1 significantly reduced mortality induced by a single dose of Dox. One of the most serious side effects of chemotherapy is myelosuppression, which can lead to blood cell deficiencies. We designed a mouse model of Dox-induced chemotoxicity (Figure 7B). We observed that Dox treatment resulted in a dramatic decrease in white blood cells and lymphocytes, whereas co-treatment with MFP M1 significantly protected mice from Dox-induced blood cell deficiencies (Figure 7C). Since ferroptosis was reported as a contributor to Dox-induced cardiac injury, we investigated whether the

**Figure 4. NRF2 is required for the upregulation of FSP1 induced by defects in mitochondrial dynamics homeostasis**

(A–C) NRF2 inhibitor ML385 rescues the sensitivity to the lipid peroxidation and ferroptosis in DRP1-KD cells, OPA1-OE cells, or MFN1-KO cells.

(A) NT AC16 cells and DRP1-KD AC16 cells were treated with erastin (20 μM) with or without ML385 (10 μM) for 16 h for cell death measurement or 12 h for lipid ROS measurement.

(B) Vector control and OPA1-OE AC16 cells were treated with erastin (20 μM) with or without ML385 (10 μM) for 16 h for cell death measurement or 12 h for lipid ROS measurement.

(C) Control cells and MFN1-KO cells in MEFs were treated with erastin (10 μM) with or without ML385 (10 μM) for 8 h for cell death measurement or 6 h for lipid ROS measurement.

(D–F) The upregulation of FSP1 is blocked by ML385 treatment.

(D) Top: western blot analysis of FSP1 expression in NT AC16 cells and DRP1-KD AC16 cells treated with ML385 (10 μM) for 12 h. Bottom: quantity analysis of FSP1 expression.

(E) Top: western blot analysis of FSP1 expression in vector control and OPA1-OE AC16 cells treated with ML385 (10 μM) for 12 h. Bottom: quantity analysis of FSP1 expression.

(F) Top: western blot analysis of FSP1 expression in control cells and MFN1-KO cells treated with ML385 (10 μM) for 12 h in MEFs. Bottom: quantity analysis of FSP1 expression.

(G) KD of NRF2 in DRP1-KD cells restores the sensitivity to lipid peroxidation and ferroptosis. AC16 cells as indicated were treated with erastin (20 μM) for 16 h for cell death measurement or 12 h for lipid ROS measurement.

(H) KD of NRF2 in OPA1-OE cells restores the sensitivity to lipid peroxidation and ferroptosis. AC16 cells as indicated were treated with erastin (20 μM) for 16 h for cell death measurement or 12 h for lipid ROS measurement.

(I) KD of NRF2 in MFN1-KD MEFs restores the sensitivity to lipid peroxidation and ferroptosis. MEFs as indicated were treated with erastin (10 μM) for 8 h for cell death measurement or 6 h for lipid ROS measurement.

(J) KD of NRF2 blocked the upregulation of FSP1 protein in DRP1-KD cells. Western blot analysis of FSP1 expression in AC16 cells as indicated.

(K) KD of NRF2 blocked the upregulation of FSP1 protein in OPA1-OE cells. Western blot analysis of FSP1 expression in AC16 cells as indicated.

(L) KD of NRF2 blocked the upregulation of FSP1 protein in MFN1-KD cells. Western blot analysis of FSP1 expression in MEFs as indicated.

All quantitative data are presented as mean ± SD from three independent experiments, and $p$ values were calculated with an unpaired t test (*$p < 0.05$, **$p < 0.01$, ***$p < 0.001$, and ****$p < 0.0001$).

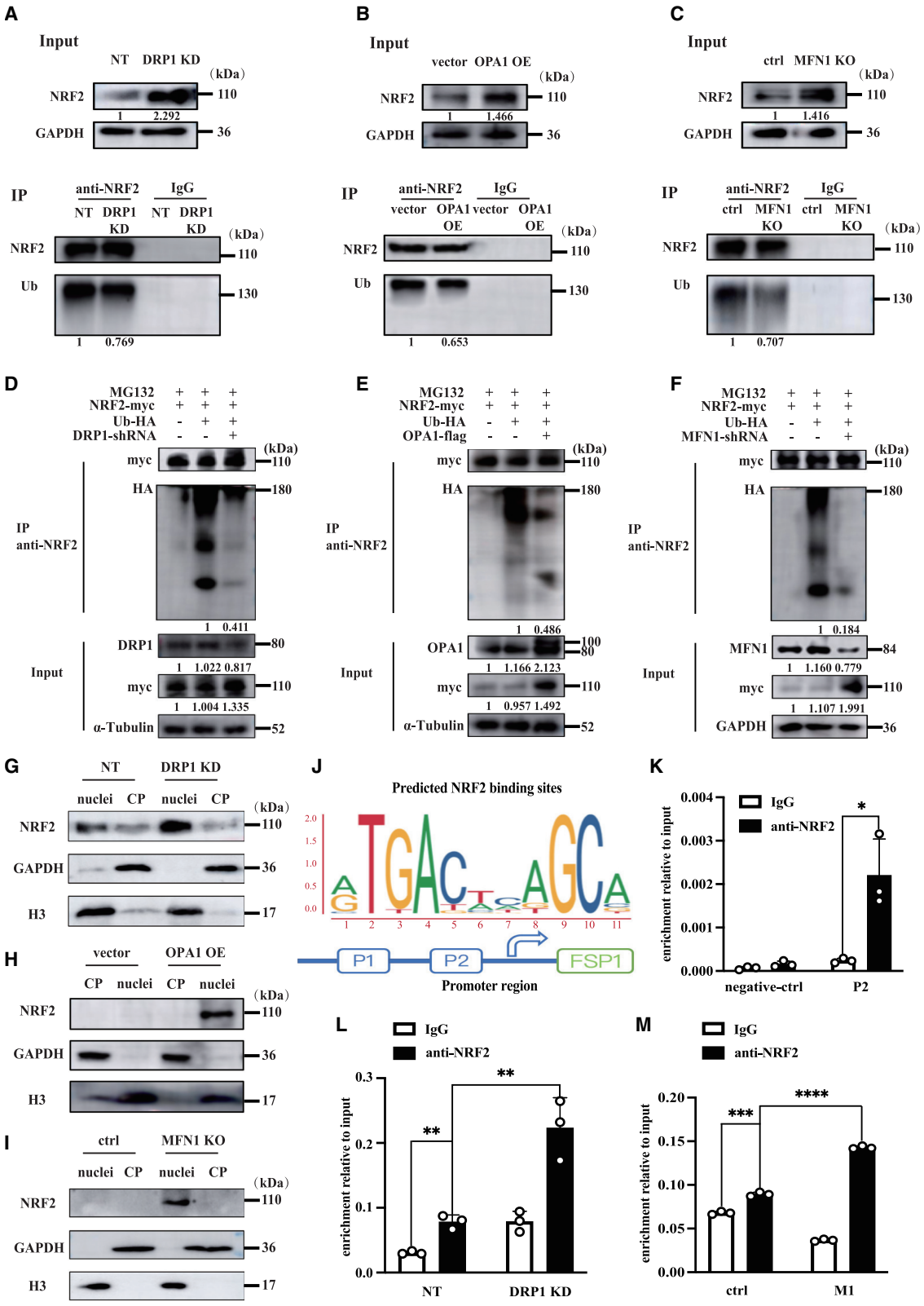


*(legend on next page)*

disturbance of mitochondrial dynamics homeostasis effectively protects heart function from Dox-induced chemotoxicity. The mice were subjected to Dox plus MFP M1 or Dox alone, and their heart function was measured by echocardiography. Co-treatment with MFP M1 significantly improved heart function, as evidenced by echocardiograms (Figure 7D). We further performed a histological examination and found that MFP M1 co-treatment alleviated Dox-induced cardiomyopathy (Figure 7E). The functional improvement of animal hearts co-treated with MFP M1 was accompanied by a blockage of Dox-induced upregulation of Anp and Myh7 mRNA levels, two classic biomarkers of cardiac hypertrophy (Figure 7F). We also detected the ability of MFP M1 to protect against Dox-induced cell death by measuring the plasma level of aspartate transaminase (AST) and lactate dehydrogenase (LDH) (Figure 7G). We further assessed mitochondria in the hearts of DOX-treated mice using transmission electron microscopy. Our analysis revealed that the myocardial mitochondria in DOX-treated mice were severely distorted and that these DOX-induced effects were rescued by MFP M1 co-treatment (Figure 7H). Consistently, Dox treatment suppressed the expression of FSP1, and MFP M1 co-treatment resulted in the significant upregulation of FSP1 in the heart tissue at both the protein level (Figure 7I) and the mRNA level (Figure 7J). Dox treatment also induced a significant increase in 4-hydroxynonenal (4-HNE) (Figure 7I) and PTGS2 (Figure 7K), two markers of ferroptosis. Finally, we used two cancer models, a mouse melanoma cell B16-derived xenograft mouse model (Figures S7A–S7C) and a human kidney cancer cell ACHN-derived xenograft mouse model (Figures S7D–S7F), to assess whether MFP M1 attenuates the ability of Dox to treat malignancies. As shown in Figure S4, MFP M1 co-treatment did not reduce the anti-tumor efficacy of Dox in either animal model, suggesting that MFP M1 might be a potential drug to mitigate the adverse side effects of Dox.

## DISCUSSION

Collectively, our study uncovered the importance of mitochondrial dynamics homeostasis on ferroptosis. The crucial role of the canonical metabolism function of mitochondria in ferroptosis has been well appreciated. A functional mitochondrial citric acid cycle and its downstream oxidative phosphorylation are required for ferroptosis. The continuous dynamic change of mitochondrial shape by fusion and fission events is critical to maintain mitochondrial quality and function in response to challenges in energy and stress. In this study, we found that ferroptosis inducer treatment results in dramatic mitochondrial fragmentation. The blockage of mitochondrial fragmentation by genetic depletion or a small-molecular inhibitor of DRP1 significantly inhibits lipid peroxidation and ferroptosis, which has also been observed recently by other groups.[47,48] Consistently, promoting mitochondrial fusion with small-molecular MFP1 or overexpression of OPA1 could suppress ferroptosis. Unexpectedly, we found that inhibition of mitochondrial fusion by the depletion of MFN1/2 or OPA1 could also block lipid peroxidation and ferroptosis. Hence, our data suggest that maintaining a functional mitochondrial dynamic homeostasis is required for ferroptosis.

FSP1, an oxidoreductase that utilizes NADPH to reduce CoQ to $CoQH_2$, plays an essential role in the inhibition of ferroptosis, parallel to GPX4. We found that disturbance of mitochondrial dynamics homeostasis by depleting mitochondrial dynamics machine proteins results in the upregulation of FSP1 on the cell membrane, which helps protect from lipid peroxidation-driven ferroptosis. Depletion of FSP1 in DRP1-KD, OPA1-OE, or MFN1-KO cells rescues ferroptosis sensitivity. NRF2 is a transcription factor that integrates cellular stress signals and responds by directing various transcriptional programs. NRF2 is upregulated upon ferroptosis stimuli treatment and negatively regulates ferroptosis by promoting multiple antioxidant proteins expression. Here, we found that the upregulation of FSP1 requires NRF2. Pharmacological inhibition or genetic depletion of NRF2 in mitochondrial dynamics-defected cells inhibits the up-expression of FSP1 and sensitizes cells to ferroptosis. Interestingly, consistent with a previous study,[49] we also noticed that the pharmacological inhibition of NRF2 in control AC16 cells cannot suppress the expression of FSP1, suggesting that the expression of FSP1 is regulated in a NRF2-dependent and -independent manner.

Mitochondria are the central powerhouses of cellular energy. We found that disruption of mitochondrial dynamics homeostasis results in the decrease of ATP and the increase of the ratio of [AMP +ADP]/[ATP], which further activates the master energy sensor

**Figure 5. Defects in mitochondrial dynamics homeostasis stabilize NRF2 and promote accumulation of NRF2 in the nucleus, and NRF2 triggers the upregulation of FSP1**

(A–C) Western analysis of the expression (input) and ubiquitination (IP) of NRF2 in DRP1-KD AC16 cells (A), OPA1-OE AC16 cells (B), or MFN1-KO MEFs (C). IP assay was performed with the antibody against NRF2 or immunoglobulin (Ig)G control using indicated AC16 cell lysate, and the ubiquitinated NRF2 was determined with the antibody against ubiquitin (Ub).

(D–F) Western blot analysis of the expression (input) and ubiquitination (IP) of NRF2 in DRP1-KD (D), OPA1-OE (E), or MFN1-KD (F) HEK293T cells. 5 μg indicated plasmids were transfected in HEK293T cells and MG132 (10 μM) was given as treatment to transfected HEK293T cells for 6 h before IP assay. IP assay was performed with the antibody against NRF2 using indicated HEK293T cell lysate, and the ubiquitinated NRF2 was determined with the hemagglutinin (HA) antibody to detect Ub-HA.

(G–I) Western blot analysis of the nuclear accumulation of NRF2 in DRP1-KD AC16 cells (G), OPA1-OE AC16 cells (H), or MFN1-KO MEFs (I). GAPDH: the biomarker of cytoplasm (CP) and H3: the biomarker of nuclei.

(J) Putative NRF2 binding sites on the promoter region of FSP1.

(K) Chromatin-IP assay of the binding of NRF2 on the promoter region of FSP1. The enrichment relative to input in wild-type HepG2 cells was measured by chromatin-IP assay. 25 μg chromatin was used as input, and 1 μL of 20 μL chromatin was used as template as qPCR.

(L and M) Chromatin-IP assay analysis of the NRF2 binding at the P2 site on the promoter region of FSP1 in DRP1-KD HepG2 cells (L) or HepG2 cells with MPF M1 treatment (M).

All quantitative data are presented as mean ± SD from three independent experiments, and $p$ values were calculated with an unpaired t test (*$p < 0.05$, **$p < 0.01$, ***$p < 0.001$, and ****$p < 0.0001$).

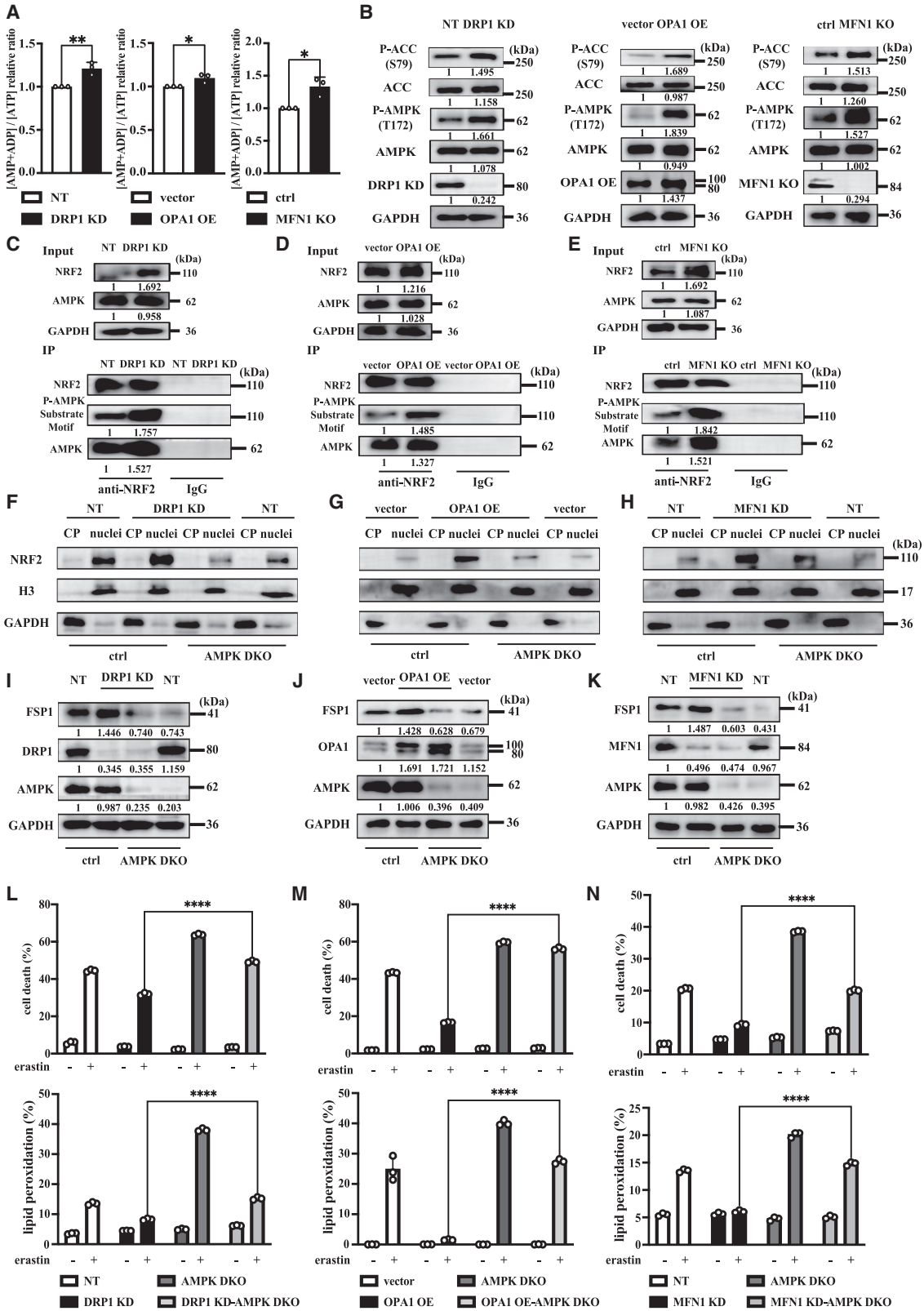


*(legend on next page)*

AMPK. The Gan lab and our lab previously reported that the activation of AMPK by energy stress suppresses ferroptosis by inhibiting lipid synthesis.[27,33] Both studies demonstrated that AMPK modulates ferroptosis, at least in part, by phosphorylating and inactivating ACC, thereby influencing lipid metabolism. AMPK-mediated ACC phosphorylation and inactivation suppress the conversion of acetyl-coenzyme A (CoA) to malonyl-CoA, a critical step in fatty acid biosynthesis—including long-chain PUFAs. This inhibition reduces lipid peroxide accumulation, ultimately attenuating ferroptosis. We found here that AMPK phosphorylates NRF2 and promotes the accumulation of NRF2 in the nucleus. NRF2 binds to the promoter region of FSP1 and regulates FSP1 expression, thus negatively regulating ferroptosis. Interestingly, the disruption of mitochondrial dynamics homeostasis activates AMPK, which further phosphorylates and inactivates ACC, suggesting that mitochondrial dysfunction negatively regulates ferroptosis in part by inhibiting the biosynthesis of fatty acids. We also observed that glucose starvation can promote NRF2 nuclear accumulation and upregulate FSP1 expression (Figure S6G). Further studies should be performed to systemically investigate additional pathways that may be involved in AMPK-mediated regulation of ferroptosis.

Chemotherapy is one of the most common approaches to treating cancer. However, chemotherapy treatment also carries a risk of side effects. The crucial role of ferroptosis in cardiovascular disease has been reported, and ferroptosis could be a target for protection against cardiomyopathy. Here, we identified that a mitochondrial fusion promoter, MFP M1, as a ferroptosis suppressor, could protect animals against Dox-induced chemotoxicity without compromising the anti-tumor efficiency of Dox.

### Limitations of the study

Our current study provides valuable insights into the role of mitochondrial dynamics in ferroptosis and may contribute to future therapeutic development. However, several unresolved issues remain to be explored further. First, while we have demonstrated that the disruption of mitochondrial dynamics upregulates NRF2-mediated FSP1 expression and inhibits ferroptosis. We could not rule out that the disruption of mitochondrial dynamics can also change the expression of other ferroptosis regulators. Other mechanisms, independent of FSP1, that contribute to ferroptosis resistance under mitochondrial stress should be further studied. Second, this study uncovered that the disruption of mitochondrial dynamics impairs ATP generation by downregulating mitochondrial ETC proteins; however, the detailed mechanism should be further investigated. Finally, we identified MFP M1 as a ferroptosis suppressor that could protect mice against Dox-induced chemotoxicity without compromising the anti-tumor efficiency of Dox. While mouse models offer valuable mechanistic insights, translating these findings to human patients requires further investigation.

## RESOURCE AVAILABILITY

### Lead contact

Further information and requests for resources and reagents should be directed to and will be fulfilled by the lead contact, Minghui Gao (gaominghui@hit.edu.cn).

### Materials availability

This study did not generate new, unique reagents.

### Data and code availability

- All data associated with this study are available in the main text or the supplemental information.
- This study did not generate any original code.
- Any additional information required to reanalyze the data reported in this paper is available from the lead contact upon request.

## ACKNOWLEDGMENTS

The authors thank members of the Gao lab for critical reading and suggestions. This work is supported by the National Natural Science Foundation of China (31871388 to M.G.), the Heilongjiang Natural Science Foundation (YQ2020C031 to M.G.), and Harbin Institute of Technology funding (to M.G.).

## AUTHOR CONTRIBUTIONS

Conceptualization, M.G. and W.Z.; methodology, S.M. and J.Q.; investigation, S.M., J.Q., Y.Z., J.L., N.S., G.H., J.H., and Y.X.; writing – original draft, S.M. and M.G.; writing – review & editing, S.M., J.Q., Y.Z., J.L., N.S., G.H., J.H., Y.X., W.Z., and M.G.; funding acquisition, M.G.; and supervision, M.G. and W. Z.

## DECLARATION OF INTERESTS

S.M., J.Q., and M.G. have a patent application related to this study.

## DECLARATION OF GENERATIVE AI AND AI-ASSISTED TECHNOLOGIES IN THE WRITING PROCESS

During the preparation of this work, the authors used Kimi.AI in order to polish the written English. After using this tool/service, the authors reviewed and

**Figure 6. Phosphorylation of NRF2 by AMPK is required for NRF2 nuclear accumulation, FSP1 upregulation, and ferroptosis resistance in mitochondrial dynamics-defected cells**

(A) Analysis of the levels of AMP, ADP, and ATP in indicated cells using the ATP, ADP, and AMP assay kit coupled with high-performance liquid chromatography (HPLC) analysis. The ratio of [AMP+ADP]/[ATP] is shown.

(B) Western blot analysis of the phosphorylation of $AMPK^{T172}$ and $ACC^{S79}$ in indicated cells.

(C–E) IP assay analysis of the phosphorylation of NRF2 and the interaction between NRF2 and AMPK in DRP1-KD AC16 cells (C), OPA1-OE AC16 cells (D), and MFN1-KO MEFs (E).

(F–H) Western blot analysis of the NRF2 accumulation in nuclei of DRP1-KD/AMPK-double KO (DKO) (F), OPA1-OE/AMPK-DKO (G), and MFN1-KD/AMPK-DKO (H) MEFs by separation of nuclear and cytoplasmic protein assay.

(I–K) Western blot analysis of the protein level of FSP1 in DRP1-KD/AMPK-DKO (I), OPA1-OE/AMPK-DKO (J), and MFN1-KD/AMPK-DKO MEFs (K).

(L–N) Depletion of AMPK in DRP1-KD MEFs (L), OPA1-OE MEFs (M), or MFN1-KD MEFs (N) rescued the sensitivity to lipid peroxidation and ferroptosis. MEFs as indicated were treated with erastin (10 μM) for 8 h for cell death measurement or 6 h for lipid ROS measurement.

All quantitative data are presented as mean ± SD from three independent experiments, and $p$ values were calculated with an unpaired t test (*$p < 0.05$, **$p < 0.01$, ***$p < 0.001$, and ****$p < 0.0001$).

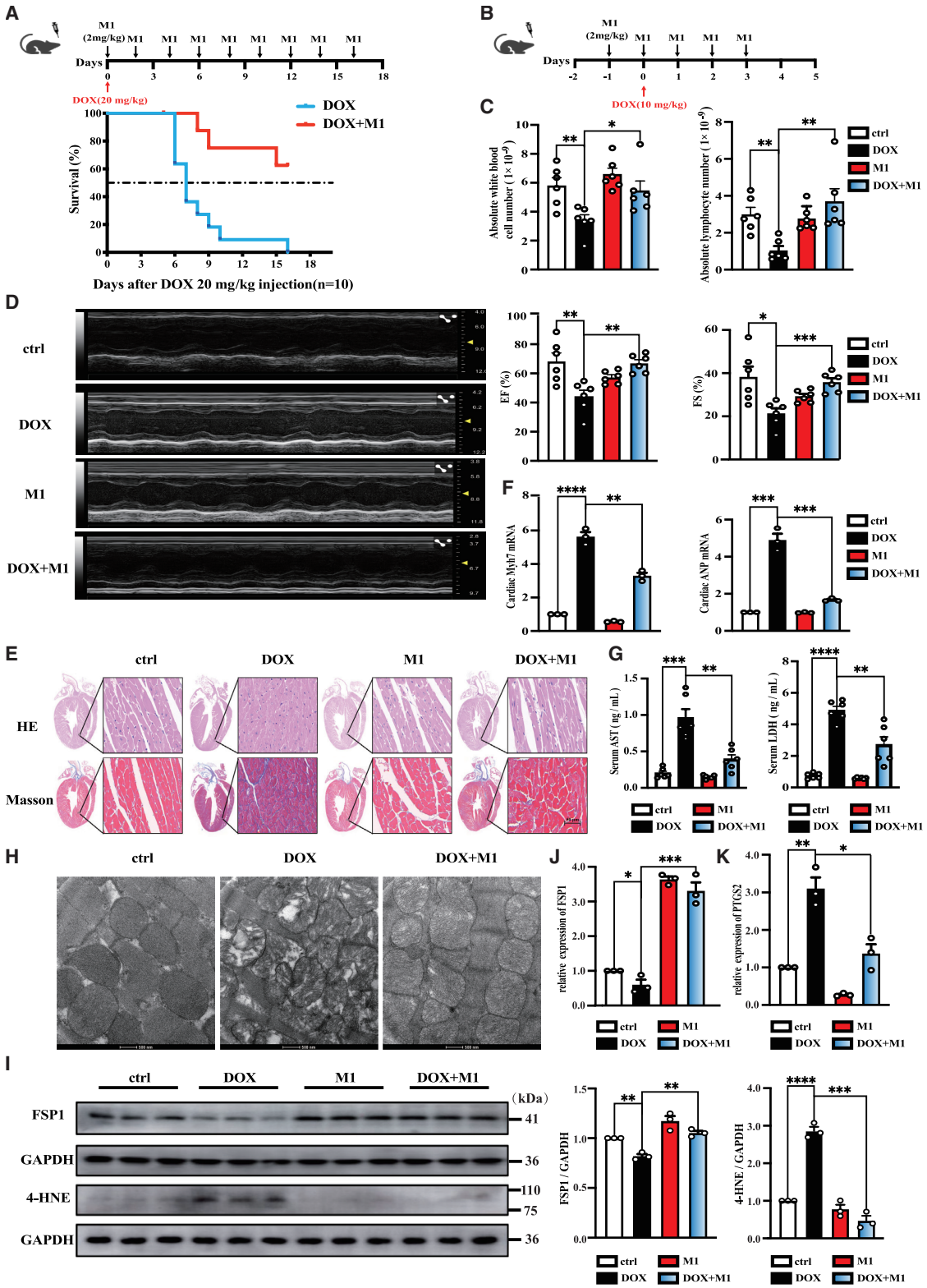


**Figure 7. MFP M1 protects against doxorubicin-induced chemotoxicity**

(A) MFP M1 reduces the mortality induced a single dose of doxorubicin (Dox). 8-week-old C57 male mice were intraperitoneally (i.p.) injected with 2 mg/kg MFP M1 (dissolved in 5% DMSO + 10% PEG300) 4 h before Dox (20 mg/kg) treatment, and then MFP M1 was injected once every 2 days for 16 days as indicated.

*(legend continued on next page)*

edited the content as needed and take full responsibility for the content of the publication.

## STAR★METHODS

Detailed methods are provided in the online version of this paper and include the following:

- KEY RESOURCES TABLE
- EXPERIMENTAL MODEL AND STUDY PARTICIPANT DETAILS
  - Mice model
  - Cell culture
- METHOD DETAILS
  - Measurement of lipid ROS, total ROS and mitochondrial ROS
  - Generation of stable cells
  - Fluorescence microscopy
  - Separation of mitochondria and plasma membrane
  - Separation of nuclear and cytoplasmic protein
  - Chromatin immunoprecipitation assay
  - IP assay
  - RT–qPCR
  - The ubiquitination assay
  - Measurement of AMP, ADP, and ATP content
  - Mice drug treatment
  - Echocardiography
  - HE staining
  - Masson staining
  - Transmission electron microscopy
  - Xenograft mouse model
  - Statistical analysis

## SUPPLEMENTAL INFORMATION

Supplemental information can be found online at https://doi.org/10.1016/j.celrep.2025.116234.

Received: March 12, 2025
Revised: July 3, 2025
Accepted: August 12, 2025
Published: September 3, 2025

## REFERENCES

1. Angeli, J.P.F., Shah, R., Pratt, D.A., and Conrad, M. (2017). Ferroptosis Inhibition: Mechanisms and Opportunities. Trends Pharmacol. Sci. *38*, 489–498. https://doi.org/10.1016/j.tips.2017.02.005.
2. Gao, M., and Jiang, X. (2018). To eat or not to eat-the metabolic flavor of ferroptosis. Curr. Opin. Cell Biol. *51*, 58–64. https://doi.org/10.1016/j.ceb.2017.11.001.
3. Stockwell, B.R., Friedmann Angeli, J.P., Bayir, H., Bush, A.I., Conrad, M., Dixon, S.J., Fulda, S., Gascón, S., Hatzios, S.K., Kagan, V.E., et al. (2017). Ferroptosis: A Regulated Cell Death Nexus Linking Metabolism, Redox Biology, and Disease. Cell *171*, 273–285. https://doi.org/10.1016/j.cell.2017.09.021.
4. Xie, Y., Hou, W., Song, X., Yu, Y., Huang, J., Sun, X., Kang, R., and Tang, D. (2016). Ferroptosis: process and function. Cell Death Differ. *23*, 369–379. https://doi.org/10.1038/cdd.2015.158.
5. Dixon, S.J., Lemberg, K.M., Lamprecht, M.R., Skouta, R., Zaitsev, E.M., Gleason, C.E., Patel, D.N., Bauer, A.J., Cantley, A.M., Yang, W.S., et al. (2012). Ferroptosis: An Iron-Dependent Form of Nonapoptotic Cell Death. Cell *149*, 1060–1072. https://doi.org/10.1016/j.cell.2012.03.042.
6. Yang, W.S., SriRamaratnam, R., Welsch, M.E., Shimada, K., Skouta, R., Viswanathan, V.S., Cheah, J.H., Clemons, P.A., Shamji, A.F., Clish, C.B., et al. (2014). Regulation of ferroptotic cancer cell death by GPX4. Cell *156*, 317–331. https://doi.org/10.1016/j.cell.2013.12.010.
7. Friedmann Angeli, J.P., Schneider, M., Proneth, B., Tyurina, Y.Y., Tyurin, V.A., Hammond, V.J., Herbach, N., Aichler, M., Walch, A., Eggenhofer, E., et al. (2014). Inactivation of the ferroptosis regulator Gpx4 triggers acute renal failure in mice. Nat. Cell Biol. *16*, 1180–1191. https://doi.org/10.1038/ncb3064.
8. Ingold, I., Berndt, C., Schmitt, S., Doll, S., Poschmann, G., Buday, K., Roveri, A., Peng, X., Porto Freitas, F., Seibt, T., et al. (2018). Selenium Utilization by GPX4 Is Required to Prevent Hydroperoxide-Induced Ferroptosis. Cell *172*, 409–422.e21. https://doi.org/10.1016/j.cell.2017.11.048.
9. Bersuker, K., Hendricks, J.M., Li, Z., Magtanong, L., Ford, B., Tang, P.H., Roberts, M.A., Tong, B., Maimone, T.J., Zoncu, R., et al. (2019). The CoQ oxidoreductase FSP1 acts parallel to GPX4 to inhibit ferroptosis. Nature *575*, 688–692. https://doi.org/10.1038/s41586-019-1705-2.
10. Doll, S., Freitas, F.P., Shah, R., Aldrovandi, M., da Silva, M.C., Ingold, I., Goya Grocin, A., Xavier da Silva, T.N., Panzilius, E., Scheel, C.H., et al. (2019). FSP1 is a glutathione-independent ferroptosis suppressor. Nature *575*, 693–698. https://doi.org/10.1038/s41586-019-1707-0.
11. Gao, M., Monian, P., Quadri, N., Ramasamy, R., and Jiang, X. (2015). Glutaminolysis and Transferrin Regulate Ferroptosis. Mol. Cell *59*, 298–308. https://doi.org/10.1016/j.molcel.2015.06.011.
12. Linkermann, A., Skouta, R., Himmerkus, N., Mulay, S.R., Dewitz, C., De Zen, F., Prokai, A., Zuchtriegel, G., Krombach, F., Welz, P.S., et al. (2014). Synchronized renal tubular cell death involves ferroptosis. Proc. Natl. Acad. Sci. USA *111*, 16836–16841. https://doi.org/10.1073/pnas.1415518111.

(B) Schematic illustration of the experimental design of Dox-induced chemotoxicity in mouse model. 8-week-old C57 male mice were i.p. injected with 2 mg/kg MFP M1 (dissolved in 5% DMSO + 10% PEG300) 24 and 4 h before Dox (10 mg/kg) treatment, and then MFP M1 was injected once every day for 3 days as indicated.
(C) MFP M1 protects mice against Dox-induced blood cell deficiencies.
(D–F) MFP M1 treatment improves Dox-induced heart injury.
(D) Mice were injected with one dose of Dox with or without MFP M1 as indicated in (B). After being anesthetized with tribromoethanol, animal heart function was measured by echocardiograms.
(E) Histological examination showed that MFP M1 co-treatment alleviated Dox-induced cardiomyopathy. Mouse were treated as in (B), and hearts were harvested and stained with H&E staining and Masson staining. Scale bars in images of all figures represent 50 μm.
(F) MFP M1 treatment blocks Dox-induced upregulation of Anp and Myh7. Mice were injected with Dox plus MFP M1 or Dox alone as indicated in (B). Total RNA isolated from mice hearts was used to measure the expression level of Anp and Myh7.
(G) MFP M1 treatment blocks increase of plasma aspartate transaminase (AST) and plasma lactate dehydrogenase (LDH) induced by Dox.
(H) MFP M1 protects against Dox-induced injury of cardiac mitochondria. Mice were treated with Dox with MFP M1 or Dox alone as indicated in (B). Scale bars in images of all figures represent 500 nm.
(I) MFP1 co-treatment blocks Dox-induced downregulation of FSP1 and upregulation of 4-HNE.
(J) MFP1 treatment increases the mRNA of FSP1.
(K) MFP1 co-treatment suppresses Dox-induced upregulation of PTGS2 mRNA.
All quantitative data are presented as mean ± SD from independent experiments, and $p$ values were calculated with an unpaired t test ($n = 6$; $^{*}p < 0.05$, $^{**}p < 0.01$, $^{***}p < 0.001$, and $^{****}p < 0.0001$).

13. Alim, I., Caulfield, J.T., Chen, Y., Swarup, V., Geschwind, D.H., Ivanova, E., Seravalli, J., Ai, Y., Sansing, L.H., Ste Marie, E.J., et al. (2019). Selenium Drives a Transcriptional Adaptive Program to Block Ferroptosis and Treat Stroke. Cell *177*, 1262–1279.e25. https://doi.org/10.1016/j.cell.2019.03.032.

14. Fang, X., Wang, H., Han, D., Xie, E., Yang, X., Wei, J., Gu, S., Gao, F., Zhu, N., Yin, X., et al. (2019). Ferroptosis as a target for protection against cardiomyopathy. Proc. Natl. Acad. Sci. USA *116*, 2672–2680. https://doi.org/10.1073/pnas.1821022116.

15. Skouta, R., Dixon, S.J., Wang, J., Dunn, D.E., Orman, M., Shimada, K., Rosenberg, P.A., Lo, D.C., Weinberg, J.M., Linkermann, A., and Stockwell, B.R. (2014). Ferrostatins Inhibit Oxidative Lipid Damage and Cell Death in Diverse Disease Models. J. Am. Chem. Soc. *136*, 4551–4556. https://doi.org/10.1021/ja411006a.

16. Chen, L., Hambright, W.S., Na, R., and Ran, Q. (2015). Ablation of the Ferroptosis Inhibitor Glutathione Peroxidase 4 in Neurons Results in Rapid Motor Neuron Degeneration and Paralysis. J. Biol. Chem. *290*, 28097–28106. https://doi.org/10.1074/jbc.M115.680090.

17. Jiang, L., Kon, N., Li, T., Wang, S.J., Su, T., Hibshoosh, H., Baer, R., and Gu, W. (2015). Ferroptosis as a p53-mediated activity during tumour suppression. Nature *520*, 57–62. https://doi.org/10.1038/Nature14344.

18. Galluzzi, L., Bravo-San Pedro, J.M., and Kroemer, G. (2015). Ferroptosis in p53-dependent oncosuppression and organismal homeostasis. Cell Death Differ. *22*, 1237–1238. https://doi.org/10.1038/cdd.2015.54.

19. Jennis, M., Kung, C.P., Basu, S., Budina-Kolomets, A., Leu, J.I.J., Khaku, S., Scott, J.P., Cai, K.Q., Campbell, M.R., Porter, D.K., et al. (2016). An African-specific polymorphism in the TP53 gene impairs p53 tumor suppressor function in a mouse model. Genes Dev. *30*, 918–930. https://doi.org/10.1101/gad.275891.115.

20. Wang, S.J., Li, D., Ou, Y., Jiang, L., Chen, Y., Zhao, Y., and Gu, W. (2016). Acetylation Is Crucial for p53-Mediated Ferroptosis and Tumor Suppression. Cell Rep. *17*, 366–373. https://doi.org/10.1016/j.celrep.2016.09.022.

21. Zhang, Y., Shi, J., Liu, X., Feng, L., Gong, Z., Koppula, P., Sirohi, K., Li, X., Wei, Y., Lee, H., et al. (2018). BAP1 links metabolic regulation of ferroptosis to tumour suppression. Nat. Cell Biol. *20*, 1181–1192. https://doi.org/10.1038/s41556-018-0178-0.

22. Zhang, Y., Zhuang, L., and Gan, B. (2019). BAP1 suppresses tumor development by inducing ferroptosis upon SLC7A11 repression. Mol. Cell. Oncol. *6*, 1536845. https://doi.org/10.1080/23723556.2018.1536845.

23. Gao, M., Yi, J., Zhu, J., Minikes, A.M., Monian, P., Thompson, C.B., and Jiang, X. (2019). Role of Mitochondria in Ferroptosis. Mol. Cell *73*, 354–363.e3. https://doi.org/10.1016/j.molcel.2018.10.042.

24. Lei, G., Zhuang, L., and Gan, B. (2024). The roles of ferroptosis in cancer: Tumor suppression, tumor microenvironment, and therapeutic interventions. Cancer Cell *42*, 513–534. https://doi.org/10.1016/j.ccell.2024.03.011.

25. Sun, N., Wang, J., Qin, J., Ma, S., Luan, J., Hou, G., Zhang, W., and Gao, M. (2024). Oncogenic RTKs sensitize cancer cells to ferroptosis via c-Myc mediated upregulation of ACSL4. Cell Death Dis. *15*, 861. https://doi.org/10.1038/s41419-024-07254-9.

26. Alborzinia, H., Flórez, A.F., Kreth, S., Brückner, L.M., Yildiz, U., Gartlgruber, M., Odoni, D.I., Poschet, G., Garbowicz, K., Shao, C., et al. (2022). MYCN mediates cysteine addiction and sensitizes neuroblastoma to ferroptosis. Nat. Cancer *3*, 471–485. https://doi.org/10.1038/s43018-022-00355-4.

27. Li, C., Dong, X., Du, W., Shi, X., Chen, K., Zhang, W., and Gao, M. (2020). LKB1-AMPK axis negatively regulates ferroptosis by inhibiting fatty acid synthesis. Signal Transduct Tar *5*, 187. https://doi.org/10.1038/s41392-020-00297-2.

28. Mao, C., Lei, G., Horbath, A., Wang, M., Lu, Z., Yan, Y., Liu, X., Kondiparthi, L., Chen, X., Cheng, J., et al. (2024). Unraveling ETC complex I function in ferroptosis reveals a potential ferroptosis-inducing therapeutic strategy for LKB1-deficient cancers. Mol. Cell *84*, 1964–1979.e6. https://doi.org/10.1016/j.molcel.2024.04.009.

29. Wang, W., Green, M., Choi, J.E., Gijón, M., Kennedy, P.D., Johnson, J.K., Liao, P., Lang, X., Kryczek, I., Sell, A., et al. (2019). CD8(+) T cells regulate tumour ferroptosis during cancer immunotherapy. Nature *569*, 270–274. https://doi.org/10.1038/s41586-019-1170-y.

30. Lang, X., Green, M.D., Wang, W., Yu, J., Choi, J.E., Jiang, L., Liao, P., Zhou, J., Zhang, Q., Dow, A., et al. (2019). Radiotherapy and immunotherapy promote tumoral lipid oxidation and ferroptosis via synergistic repression of SLC7A11. Cancer Discov. *9*, 1673–1685. https://doi.org/10.1158/2159-8290.CD-19-0338.

31. Hou, W., Xie, Y., Song, X., Sun, X., Lotze, M.T., Zeh, H.J., Kang, R., and Tang, D. (2016). Autophagy promotes ferroptosis by degradation of ferritin. Autophagy *12*, 1425–1428. https://doi.org/10.1080/15548627.2016.1187366.

32. Gao, M., Monian, P., Pan, Q., Zhang, W., Xiang, J., and Jiang, X. (2016). Ferroptosis is an autophagic cell death process. Cell Res. *26*, 1021–1032. https://doi.org/10.1038/cr.2016.95.

33. Lee, H., Zandkarimi, F., Zhang, Y., Meena, J.K., Kim, J., Zhuang, L., Tyagi, S., Ma, L., Westbrook, T.F., Steinberg, G.R., et al. (2020). Energy-stress-mediated AMPK activation inhibits ferroptosis. Nat. Cell Biol. *22*, 225–234. https://doi.org/10.1038/s41556-020-0461-8.

34. Quintana-Cabrera, R., and Scorrano, L. (2023). Determinants and outcomes of mitochondrial dynamics. Mol. Cell *83*, 857–876. https://doi.org/10.1016/j.molcel.2023.02.012.

35. Dixon, S.J., Lemberg, K.M., Lamprecht, M.R., Skouta, R., Zaitsev, E.M., Gleason, C.E., Patel, D.N., Bauer, A.J., Cantley, A.M., Yang, W.S., et al. (2012). Ferroptosis: an iron-dependent form of nonapoptotic cell death. Cell *149*, 1060–1072. https://doi.org/10.1016/j.cell.2012.03.042.

36. Chan, D.C. (2020). Mitochondrial Dynamics and Its Involvement in Disease. Annu. Rev. Pathol. *15*, 235–259. https://doi.org/10.1146/annurev-pathmechdis-012419-032711.

37. Doll, S., Proneth, B., Tyurina, Y.Y., Panzilius, E., Kobayashi, S., Ingold, I., Irmler, M., Beckers, J., Aichler, M., Walch, A., et al. (2017). ACSL4 dictates ferroptosis sensitivity by shaping cellular lipid composition. Nat. Chem. Biol. *13*, 91–98. https://doi.org/10.1038/nchembio.2239.

38. Smirnova, E., Shurland, D.L., Ryazantsev, S.N., and van der Bliek, A.M. (1998). A human dynamin-related protein controls the distribution of mitochondria. J. Cell Biol. *143*, 351–358. https://doi.org/10.1083/jcb.143.2.351.

39. Delettre, C., Lenaers, G., Griffoin, J.M., Gigarel, N., Lorenzo, C., Belenguer, P., Pelloquin, L., Grosgeorge, J., Turc-Carel, C., Perret, E., et al. (2000). Nuclear gene, encoding a mitochondrial dynamin-related protein, is mutated in dominant optic atrophy. Nat. Genet. *26*, 207–210. https://doi.org/10.1038/79936.

40. Santel, A., and Fuller, M.T. (2001). Control of mitochondrial morphology by a human mitofusin. J. Cell Sci. *114*, 867–874.

41. Chen, H., Detmer, S.A., Ewald, A.J., Griffin, E.E., Fraser, S.E., and Chan, D.C. (2003). Mitofusins Mfn1 and Mfn2 coordinately regulate mitochondrial fusion and are essential for embryonic development. J. Cell Biol. *160*, 189–200. https://doi.org/10.1083/jcb.200211046.

42. Liang, F.G., Zandkarimi, F., Lee, J., Axelrod, J.L., Pekson, R., Yoon, Y., Stockwell, B.R., and Kitsis, R.N. (2024). OPA1 promotes ferroptosis by augmenting mitochondrial ROS and suppressing an integrated stress response. Mol. Cell *84*, 3098–3114.e6. https://doi.org/10.1016/j.molcel.2024.07.020.

43. Sun, X., Ou, Z., Chen, R., Niu, X., Chen, D., Kang, R., and Tang, D. (2016). Activation of the p62-Keap1-NRF2 pathway protects against ferroptosis in hepatocellular carcinoma cells. Hepatology *63*, 173–184. https://doi.org/10.1002/hep.28251.

44. Sandelin, A., Alkema, W., Engström, P., Wasserman, W.W., and Lenhard, B. (2004). JASPAR: an open-access database for eukaryotic transcription

factor binding profiles. Nucleic Acids Res. *32*, D91–D94. https://doi.org/10.1093/nar/gkh012.

45. Joo, M.S., Kim, W.D., Lee, K.Y., Kim, J.H., Koo, J.H., and Kim, S.G. (2016). AMPK Facilitates Nuclear Accumulation of Nrf2 by Phosphorylating at Serine 550. Mol. Cell Biol. *36*, 1931–1942. https://doi.org/10.1128/Mcb.00118-16.

46. Fang, X., Wang, H., Han, D., Xie, E., Yang, X., Wei, J., Gu, S., Gao, F., Zhu, N., Yin, X., et al. (2019). Ferroptosis as a target for protection against cardiomyopathy. Proc. Natl. Acad. Sci. USA *116*, 2672–2680. https://doi.org/10.1073/pnas.1821022116.

47. Pedrera, L., Clemente, L.P., Dahlhaus, A., Nasudivar, S.L., Tishina, S., González, D.O., Stroh, J., Yapici, F.I., Singh, R.P., Grotehans, N., et al. (2025). Ferroptosis triggers mitochondrial fragmentation via Drp1 activation. Cell Death Dis. *16*, 40. https://doi.org/10.1038/s41419-024-07312-2.

48. Tang, S., Fuss, A., Fattahi, Z., and Culmsee, C. (2024). Drp1 depletion protects against ferroptotic cell death by preserving mitochondrial integrity and redox homeostasis. Cell Death Dis. *15*, 626. https://doi.org/10.1038/s41419-024-07015-8.

49. Kim, J.W., Kim, M.J., Han, T.H., Lee, J.Y., Kim, S., Kim, H., Oh, K.J., Kim, W.K., Han, B.S., Bae, K.H., et al. (2023). FSP1 confers ferroptosis resistance in KEAP1 mutant non-small cell lung carcinoma in NRF2-dependent and -independent manner. Cell Death Dis. *14*, 567. https://doi.org/10.1038/s41419-023-06070-x.

50. Wu, J., Minikes, A.M., Gao, M., Bian, H., Li, Y., Stockwell, B.R., Chen, Z.N., and Jiang, X. (2019). Intercellular interaction dictates cancer cell ferroptosis via NF2-YAP signalling. Nature *572*, 402–406. https://doi.org/10.1038/s41586-019-1426-6.

51. Graham, L., and Orenstein, J.M. (2007). Processing tissue and cells for transmission electron microscopy in diagnostic pathology and research. Nat. Protoc. *2*, 2439–2450. https://doi.org/10.1038/nprot.2007.304.

## STAR★METHODS

### KEY RESOURCES TABLE

| REAGENT or RESOURCE | SOURCE | IDENTIFIER |
|---|---|---|
| Antibodies | | |
| anti-NRF2 | Proteintech | Cat# 16396-1-AP; RRID: AB_2782956 |
| anti-NRF2 | Abcam | Cat# ab62352; RRID: AB_944418 |
| anti-NRF2 | HUABIO | Cat# HA721432; RRID: AB_3073494 |
| anti-MFN1 | Abclonal | Cat# A9880; RRID: AB_2770351 |
| anti-MFN2 | Proteintech | Cat# 12186-1-AP; RRID: AB_2266320 |
| anti-OPA1 | HUABIO | Cat# HA-722673; RRID: AB_3070618 |
| anti-DRP1 | Proteintech | Cat# 12957-1-AP; RRID: AB_2093525 |
| anti-AMPKα | CST | Cat# 5831; RRID: AB_10622186 |
| anti-Phospho-AMPKα (Thr172) | CST | Cat# 2535; RRID: AB_331250 |
| anti-FSP1 | Proteintech | Cat# 20886-1-AP; RRID: AB_2878756 |
| anti-Ubiquitin | PTM | Cat# 5798 |
| anti-Phospho-AMPK Substrate Motif | CST | Cat# 5759T; RRID: AB_10949320 |
| anti-SLC7A11 | Proteintech | Cat# 26864-1-AP; RRID: AB_2880661 |
| anti-GPX4 | Abcam | Cat# ab231174; RRID: AB_3073732 |
| anti-GPX4 | HUABIO | Cat# ET1706-45; RRID: AB_3070665 |
| anti-GAPDH | Proteintech | Cat# 60004-1-Ig; RRID: AB_2107436 |
| anti-alpha Tubulin | Proteintech | Cat# 11224-1-AP; RRID: AB_2210206 |
| anti-ATP1A1 | Proteintech | Cat# 14418-1-AP; RRID: AB_2227873 |
| anti-Tom20 | Proteintech | Cat# 11802-1-AP; RRID: AB_2207530 |
| anti-Histone H3 | Wanleibio | Cat# WL0984a |
| anti-NDUFS1 | Santa Cruz | Cat# 271387; RRID: AB_10611343 |
| anti-SDHA | Santa Cruz | Cat# 377302; RRID: AB_2904546 |
| anti-UQCRC1 | HUABIO | Cat# HA721640; RRID: AB_3072753 |
| anti-COXIV | Wanleibio | Cat# WL02203R |
| anti-ATP5B | Santa Cruz | Cat# 55597; RRID: AB_1121153 |
| anti-ACC | CST | Cat# 3676; RRID: AB_2219397 |
| anti-Phospho-ACC (S79) | CST | Cat# 3661; RRID: AB_330337 |
| Bacterial and virus strains | | |
| Stbl3 | Beyotime | Cat# D1081M |
| Chemicals, peptides, and recombinant proteins | | |
| erastin | Selleck | Cat# S7242 |
| ML385 | APE×BIO | Cat# B8300 |
| MFP M1 | MCE | Cat# 219315-22-7 |
| BODIPY C11 | Thermo Fisher | Cat# D3861 |
| ML162 | TargetMol | Cat# T8970 |
| H2DCFDA | MCE | Cat# HY-D0940 |
| MitoSOX Red | MCE | Cat# HY-D1055 |
| Doxorubicin | MCE | Cat# HY-15142 |
| Mdivi | MCE | Cat# HY-15886 |
| RSL3 | Selleck | Cat# S8155 |
| Critical commercial assays | | |
| Mitochondria Isolation Assay Kit | Beyotime | Cat# C3601 |
| Cytoplasmic Protein Extraction Kit | Beyotime | Cat# P0028 |

(*Continued on next page*)

*Continued*

| REAGENT or RESOURCE | SOURCE | IDENTIFIER |
|---|---|---|
| PCR Purification Kit | Thermo Fisher | Cat# K0702 |
| SYBR qPCR Master Mix Kit | Vazyme | Cat# Q511-03 |
| AMP, ADP and ATP Assay Kit | Solarbio | Cat# BC5114 |
| Masson Dye Solution Set | Servicebio | Cat# G1006 |
| Hematoxylin-Eosin (H&E) HD Constant Dye Kit | Servicebio | Cat# G1076 |
| **Experimental models: Cell lines** | | |
| AC16 | ATCC | Cat# CRL-3568 |
| MEFs | ATCC | Cat# CRL-2991 |
| ACHN | ATCC | Cat# CRL-1611 |
| A549 | ATCC | Cat# CCL-185 |
| HEK293T | ATCC | Cat# CRL-3216 |
| HepG2 | ATCC | Cat# HB-8065 |
| AMPK DKO MEFs | X Jiang Lab | N/A |
| **Oligonucleotides** | | |
| Primer: ChIP-negative-ctrl-F: TAAAAAGTAGAGTGGTTGGAGTGATGACG | This paper | N/A |
| Primer: ChIP-negative-ctrl-R: TCTCAGTTTTTGCCCTTATTTAATCCC | This paper | N/A |
| Primer: hFSP1-ChIP-F: CATGGTTCTGGAGGCTGGGA | This paper | N/A |
| Primer: hFSP1-ChIP-R: GTTCAAGCTCTTCCTCTCTCTCGCTC | This paper | N/A |
| Primer: hFSP1-qPCR-F: GCGTTTGAGAGCAGACTAGC | This paper | N/A |
| Primer: hFSP1-qPCR-R: CACAGTCACCAATGGCGTAG | This paper | N/A |
| Primer: hACTIN-qPCR-F: CATGTACGTTGCTATCCAGGC | This paper | N/A |
| Primer: hACTIN-qPCR-R: CTCCTTAATGTCACGCACGAT | This paper | N/A |
| Primer: mFSP1-qPCR-F: CTGCCTACCGCAGTGCATT | This paper | N/A |
| Primer: mFSP1-qPCR-R: ACGCCATCATTTCTGCCCA | This paper | N/A |
| Primer: mGAPDH-qPCR-F: ATCATCCCTGCATCCACT | This paper | N/A |
| Primer: mGAPDH-qPCR-R: ATCCACGACGGACACATT | This paper | N/A |
| Primer: MFN1 gRNA: CCTCGGTGGAGTCGATGCGGTGG | This paper | N/A |
| Primer: Ptgs2-qPCR-F: CTGCGCCTTTTCAAGGATGG | This paper | N/A |
| Primer: Ptgs2-qPCR-R: GGGGATACACCTCTCCACCA | This paper | N/A |
| Primer: Myh7-qPCR-F: GCTGAAAGCAGAAAGAGATTATC | This paper | N/A |
| Primer: Myh7-qPCR-R: TGGAGTTCTTCTCTTCTGGAG | This paper | N/A |
| Primer: Anp-qPCR-F: TCGTCTTGGCCTTTTGGCT | This paper | N/A |
| Primer: Anp-qPCR-R: TCCAGGTGGTCTAGCAGGTTCT | This paper | N/A |
| **Recombinant DNA** | | |
| SU9-GFP | Addgene | Cat# 23214 |
| NT shRNA | Addgene | Cat# 1864 |
| pLx-gRNA | Addgene | Cat# 50662 |
| pLV3-CMV-OPA1 | Miaoling | Cat# P69521 |
| pLV3-CMV-MCS | Miaoling | Cat# P53443 |
| pLV3-CMV-NRF2-myc | Miaoling | Cat# P75390 |
| pCMV-HA-Ub | Miaoling | Cat# P0554 |
| pCDNA3-T7-KEAP1 | This paper | N/A |
| pLV3-CMV-NRF2-S550A-myc | This paper | N/A |
| Mouse MFN1 gRNA: CCTCGGTGGAGTCGATGCGGTGG | This paper | N/A |
| MISSION lentiviral shRNA clones targeting human DRP1 | Sigma-Aldrich | TRCN0000318425 |
| MISSION lentiviral shRNA clones targeting human OPA1 | Sigma-Aldrich | TRCN0000082846 |
| MISSION lentiviral shRNA clones targeting human FSP1-sh1 | Sigma-Aldrich | TRCN0000064423 |

(*Continued on next page*)

*Continued*

| REAGENT or RESOURCE | SOURCE | IDENTIFIER |
|---|---|---|
| MISSION lentiviral shRNA clones targeting human FSP1-sh2 | Sigma-Aldrich | TRCN0000064424 |
| MISSION lentiviral shRNA clones targeting human FSP1-sh3 | Sigma-Aldrich | TRCN0000064426 |
| MISSION lentiviral shRNA clones targeting human NRF2-sh1 | Sigma-Aldrich | TRCN0000281950 |
| MISSION lentiviral shRNA clones targeting human NRF2-sh2 | Sigma-Aldrich | TRCN0000007555 |
| MISSION lentiviral shRNA clones targeting human MFN1 | Sigma-Aldrich | TRCN0000300765 |
| MISSION lentiviral shRNA clones targeting mouse FSP1-sh1 | Sigma-Aldrich | TRCN0000112137 |
| MISSION lentiviral shRNA clones targeting mouse FSP1-sh2 | Sigma-Aldrich | TRCN0000112139 |
| MISSION lentiviral shRNA clones targeting mouse NRF2-sh1 | Sigma-Aldrich | TRCN0000281950 |
| MISSION lentiviral shRNA clones targeting mouse NRF2-sh2 | Sigma-Aldrich | TRCN0000007555 |
| MISSION lentiviral shRNA clones targeting mouse DRP1 | Sigma-Aldrich | TRCN0000012605 |
| MISSION lentiviral shRNA clones targeting mouse MFN2 | Sigma-Aldrich | TRCN0000080610 |
| MISSION lentiviral shRNA clones targeting mouse MFN1 | Sigma-Aldrich | TRCN0000081398 |
| Software and algorithms | | |
| GraphPad Prism 8.2.1 | Graphpad | https://www.graphpad.com/updates/prism-821-release-notes |
| ImageJ 1.52k | NIH | https://imagej.net/ij/download.html |
| FlowJo 10.8.1 | BD | https://flowjo.com/docs/flowjo10/getting-acquainted/10-8-release-notes/10-8-1-release-notes |
| Chromeleon 7.3.2 | Thermo Fisher | https://knowledge1.thermofisher.com/Software_and_Downloads/Chromatography_and_Mass_Spectrometry_Software/Chromeleon/Chromeleon_7_Software_Drivers_and_Release_Notes |
| Other | | |
| DMEM (4.5 g/L glucose) | Thermo Fisher | Cat# 11995073 |
| DMEM (1 g/L glucose) | Thermo Fisher | Cat# 11885084 |

## EXPERIMENTAL MODEL AND STUDY PARTICIPANT DETAILS

### Mice model

All animal studies were approved by the Animal Experimental Ethics Committee of Harbin Institute of Technology. The 8-weeks old C57BL/6 male mice were purchased from Liaoning Changsheng biotechnology Co., Ltd. The 4-week-old female Babl/c-nude mice were purchased from Skbex Biotechnology Co., Ltd. All efforts were made to minimize animal suffering and to reduce the number of animals used.

### Cell culture

AC16 cells are maintained in DMEM with low glucose. All other mammalian cells are maintained in DMEM with high glucose, sodium pyruvate (1 mM), glutamine (4 mM), penicillin (100 U/ml), streptomycin (0.1 mg/mL) and 10% (v/v) FBS at 37°C and 5% $CO_2$. Cell death was analyzed by PI (100 ng/mL), Sytox (5 nM) or Hoechst (1 mg/mL) staining coupled with microscopy or flow cytometry. All cell lines used in this study were authenticated by short tandem repeat (STR) profiling and confirmed to match the reference profiles from ATCC. Mycoplasma contamination testing was performed monthly using PCR and all cell lines were confirmed to be mycoplasma-free throughout the study.

## METHOD DETAILS

### Measurement of lipid ROS, total ROS and mitochondrial ROS

Measurement was analyzed by flow cytometry: cells were seeded at a density of $3.5 \times 10^5$ per well in a 6-well dish and grow overnight in DMEM. 5 μM BODIPY C11, 10 μM H2DCFDA or 10 μM MitoSOX Red was added into cell culture medium and incubated for 30 min after indicated treatment. Excess fluorescent probe was then removed by washing the cells with PBS twice. Labeled cells were

trypsinized and resuspended in PBS plus 2% FBS. Oxidation of BODIPY C11 resulted in a shift of the fluorescence emission peak from 590 nm to 510 nm, BODIPY C11 was the probe of lipid ROS. H2DCFDA (Ex/Em = 488/525 nm) was used to detect intracellular ROS. MitoSOX Red (Ex/Em = 510/580 nm) was oxidized then bound to nucleic acids in mitochondria and produced strong red fluorescence.

### Generation of stable cells

#### *AMPK double knockout MEFs were gifts from Xuejun Jiang lab*

MFN1 knockout cells were generated using CRISPR technology. pLx-gRNA (Addgene, Cat#50662) expression plasmid encoding guide RNA was generated and co-transfected with Streptococcus pyogenes Cas9 expression plasmid and transfected into cells using Lipofectamine 2000 (Life Technologies). 24 h after the transfection, the cells were trypsinzed and about 200 cells were seeded into a 10 cm plate. After cell clones were formed and expanded, western blot was performed to screening for knockout clones.

MISSION lentiviral shRNA clones were obtained from Sigma-Aldrich and expression plasmids were obtained from MiaoLing Plasmid Platform or Addgene Plasmid Platform. Retrovirus or lentivirus was packaged in 293T cells and used to infect target cells, which were then selected with puromycin or blasticidin for at least 3 days prior to use in experiments.

### Fluorescence microscopy

Cells stably expressing SU9-GFP were grown on glass cover slips in a 6-well plate. 24 h later, cells were treated as indicated. Cover slips were then fixed with 3.7% (vol/vol) paraformaldehyde (PFA) in 20 mM HEPES pH 7.5 for 30 min at room temperature. Cover slips were then mounted on microscope slides for visualization using ZEISS LSM880 with fast Airyscan Microscope with a 100× magnification objective.

### Separation of mitochondria and plasma membrane

Mitochondria and cytoplasm from $2 \times 10^7$ cells treated as indicated were isolated by using Mitochondria Isolation assay kit (Beyotime, Cat#C3601) according to the manufacturer's instruction.

To get plasma membrane fraction, $2 \times 10^7$ cells were collected and lysed in cold assay buffer A (1 mM KCl, 5 mM NaCl, 3 mM $MgCl_2$, 50 mM HEPES, 1 mM DTT, 1% Proteases Inhibitor Cocktail). Cells were frozen and thawed repeatedly in liquid nitrogen for 5 times, then centrifuged at 5000 rpm for 10 min at 4°C and the supernatant was centrifuged at 12,000 rpm for 10 min at 4°C. The pellet was resuspended in cold assay buffer B (1 mM KCl, 5 mM NaCl, 3 mM $MgCl_2$, 50 mM HEPES, 1 mM DTT, 1 mM EGTA, 1% Proteases Inhibitor Cocktail) and centrifuged at 12,000 rpm for 10 min at 4°C. Resuspend pellets in cold assay buffer C (50 mM Tris-HCl, pH 7.0, 1% Protease Inhibitor Cocktail) to get plasma membrane fraction.

### Separation of nuclear and cytoplasmic protein

Nuclear and cytoplasm protein from $2 \times 10^7$ cells were isolated by using Cytoplasmic Protein Extraction Kit (Beyotime, Cat# P0028) according to the manufacturer's instruction.

### Chromatin immunoprecipitation assay

Chromatin immunoprecipitation (ChIP) assay was performed as previously.[50] Briefly, $4 \times 10^7$ HepG2 cells were crosslinked in 0.75% formaldehyde for 10 min. Glycine was added to a final concentration of 125 mM for 5 min. After washing with cold PBS, cells were collected in PBS and sonicated on an ultrasonic homogenizer on ice for 10 min at 30% power (6 pulses, 30 s on and 30 s off) to shear DNA to an average fragment size of 200–1,000 bp. 50 μL sonicated sample was removed to determine the DNA concentration and fragment size. 100 μL cell lysates were incubated overnight with 100 μL protein A/G agarose (Thermo, Cat#20421) and 5 μg anti-NRF2 antibody (abcam, Cat#EP1808Y) or IgG antibody (Biodragon, Cat#BF02008). Beads were collected, washed and treated with proteinase K for 4 h at 65°C and RNase for 1 h at 37°C. DNA was purified with a PCR purification kit (Thermo, Cat#K0702) and eluted with 20 μL $ddH_2O$. DNA fragments were assessed by quantitative PCR with reverse transcription (qRT–PCR) by using universal SYBR qPCR Master Mix Kit (Vazyme, Cat#Q511-03) using the primer sequences listed in supplemental information. Samples were normalized to input DNA.

### IP assay

Cells were lysed in IP buffer (20 mM Tris-HCl pH 8.0, 137 mM NaCl, 1% NP-40, 2 mM EDTA, 1% Proteases Inhibitor Cocktail). The $4 \times 10^3$ μg cell lysates were incubated overnight with 3 μg anti-NRF2 antibody (proteintech, Cat#16396-1-AP) or IgG antibody (Biodragon, Cat#BF02008) at 4°C. The mix of cell lysates and antibody then were incubated overnight with 25 μL protein A/G magnetic beads (MCE, Cat#HY-K0202) at 4°C. Beads were washed with IP buffer 3 times, collected with IP buffer too, then analyzed by WB assay.

### RT–qPCR

Total RNA was extracted using TRIzol reagent (Thermo Fisher, Cat# 15596026) according to the manufacturer's instructions. cDNA was synthesized using the cDNA Synthesis Kit (Takara, Cat# RR047A) according to the manufacturer's instructions. RT–qPCR was performed with universal SYBR qPCR Master Mix Kit (Vazyme, Cat#Q511-03) in a Real-Time PCR system (Applied Biosystems). Primer sequences are listed in the key resources table.

### The ubiquitination assay

To determine the ubiquitination of NRF2 in AC16 stable cells, cells were lysed in IP buffer and endogenous NRF2 was immunoprecipitated with the antibody against NRF2 or IgG control, and the IP product was immunoblotted with the antibody against Ubiquitin.

To determine the ubiquitination of NRF2 in HEK293T cells, HEK293T cells were transfected with indicated plasmids and cultured for 48 h. After treatment with MG132 (10 μM) for 6 h, cells were lysed in IP buffer and NRF2 was immunoprecipitated with the antibody against NRF2, and the IP product was immunoblotted with the HA antibody to detect Ubiquitin-HA.

### Measurement of AMP, ADP, and ATP content

$2 \times 10^8$ cells were used to measure cellular content of AMP, ADP and ATP by HPLC using the AMP, ADP and ATP assay Kit (Solarbio, Cat#BC5114) according to the manufacturer's instruction.

### Mice drug treatment

For mice survival experiments, a single intraperitoneal injection of 20 mg/kg doxorubicin (Cat#HY-15142, MCE) was administered to 8-weeks old C57BL/6 male mice. For other mice experiments, a single intraperitoneal injection of 10 mg/kg doxorubicin or vehicle was administered to 8-weeks old C57BL/6 male mice. To test the effect of MFP M1 on doxorubicin induced toxicity, 2 mg/kg MFP M1 (dissolved in 5% DMSO+10% PEG) was administered to mice once 24 h and 4 h before doxorubicin treatment, and then once every 24 h after doxorubicin treatment.

### Echocardiography

The mice were anesthetized with tribromoethanol. Left ventricle were measured using a vevo3100 uhf imaging system with an mx400 (30MHz) probe on a 37°C heating table. Dimensions were measured in end-diastole (LVEDD) and end-systole (LVESD).

### HE staining

The paraffin sections were immersed in sequence in Environmental Friendly Dewaxing Transparent Liquid I and II for dewaxing and hydration. The frozen sections were removed from the −20°C refrigerator and restored to room temperature, fixed with tissue fixating solution for 15 min, and then rinsed with running water. The sections were then treated with HD constant staining pretreatment solution for 1 min. Put sections into Hematoxylin solution for 3–5 min. Then treat the section with Hematoxylin Differentiation solution, Hematoxylin Bluing solution. Place the sections in 95% ethanol for 1 min, Eosin dye for 15 s. Finally, dehydration and sealing.

### Masson staining

Dewaxing, hydration, rewarming and fixing are same as in the HE staining. The slices were then soaked in Masson A overnight. Masson B and Masson C were prepared into Masson solution according to the ratio of 1:1. Then stain with Masson solution for 1 min, rinse with water. Differentiate with 1% hydrochloric acid alcohol for several seconds, rinse with water.

Soak the slices in Masson D for 6 min, Masson E for 1 min, slightly drain directly into Masson F for 2-30s. Rinse the slices with 1% glacial acetic acid and then dehydration with two cups of anhydrous ethanol. Clearing and sealing: slides were soaked in 100% ethanol for 5 min; Xylene for 5 min; finally sealed with neutral gum.

### Transmission electron microscopy

A sample of myocardial tissue was fixed in 3% phosphate-glutaraldehyde and then prepared according to the protocol.[51] 5 viewing fields of each sample was randomly selected for imaging using Tecnai 20 (100 kv) transmission electron microscope (FEI).

### Xenograft mouse model

$2 \times 10^6$ ACHN human kidney cancer cells were suspended in 100 μL PBS and injected subcutaneously into 4-week-old female Babl/c-nude mouse. Tumor volume was measured every 2 days and calculated as length×(width).[2] When the tumor reached 25mm$^3$, 3 mg/kg doxorubicin was administered twice every third day, while MFP M1(2mg/kg) treatment was administered for a week. Tumor weight was measured on 28th day after mouse was scarified.

$1 \times 10^6$ B16 mouse melanoma cells were suspended in 100 μL PBS and injected subcutaneously into 6-week-old male C57BL/6 mouse. Tumor was measured every day and volume was calculated as length×(width)$^2$. When the tumor volume reached 25mm$^3$, 5 mg/kg doxorubicin was administered twice every third days, while MFP M1(2mg/kg) treatment was administered for a week. Tumor weight was measured on 28th day after mice were scarified.

### Statistical analysis

All statistical analyses were performed using Prism 5.0c GraphPad Software. $p$ values were calculated with unpaired Student's $t$-test. Data are presented as mean ± SEM from 3 independent experiments. $p < 0.05$ was set as the threshold for significance (*$p < 0.05$, **$p < 0.01$, ***$p < 0.001$, ****$p < 0.0001$, ns: no significance).

**Cell Reports, Volume *44***

## Supplemental information

# Disrupting mitochondrial dynamics attenuates ferroptosis and chemotoxicity via upregulating NRF2-mediated FSP1 expression

**Shuang Ma, Jianhua Qin, Yao Zhang, Jing Luan, Na Sun, Guoyuan Hou, Jiyuan He, Yang Xiao, Wei Zhang, and Minghui Gao**

**Figure S1. Depletion of DRP1 and MFP M1 treatment blocks ferroptosis associated mitochondrial fragmentation.**

(**A**) NT AC16 cells and DRP1 KD AC16 cells labelled with SU9-GFP were treated with erastin (20 μM) for 0, 4, 8 h. SU9-GFP labelled mitochondria was imaged using confocal laser scanning microscope. (**B**) Wild-type AC16 cells labelled with SU9-GFP were treated with erastin (20 μM) or MFP M1 (20 μM) for 12 h. SU9-GFP labelled mitochondria was imaged using confocal laser scanning microscope. (**C**) Cell death measurement of DRP1 KD, OPA1 OE or control AC16 cells treated with RSL3 as indicated. (**D**) Cell death measurement of DRP1 KD, OPA1 OE or control AC16 cells treated with ML162 as indicated.

All quantitative data are presented as mean ± SD from three independent experiments; and P values were calculated with unpaired t test (ns: no significance). scale bars in images of all figures were 10 μM.

**Figure S2. Knockout of MFN1 cannot suppress RSL3 or ML162 induced ferroptosis.**

(**A**) Cell death measurement of MFN1 KO or control MEFs treated with RSL3 as indicated. (**B**) Cell death measurement of MFN1 KO or control MEFs treated with ML162 as indicated.

All quantitative data are presented as mean ± SD from three independent experiments; and P values were calculated with unpaired t test (ns: no significance).

**Figure S3. The mRNA of FSP1 is upregulated upon disrupting mitochondria homeostasis.**

(**A**) The mRNA level of FSP1 is upregulated in DRP1 KD cells. The relative expression of mRNA level of FSP1 in NT AC16 cells and DRP1 KD AC16 cells was assessed by real-time quantitative PCR assay. (**B**) The mRNA level of FSP1 is upregulated in OPA1 OE cells. The relative expression of mRNA level of FSP1 in vector control AC16 cells and OPA1 OE AC16 cells was assessed by real-time quantitative PCR assay. (**C**) The mRNA level of FSP1 was upregulated in MFN1 KO cells. The relative expression of mRNA level of FSP1 in control cells and MFN1 KO cells in MEFs was assessed by real-time quantitative PCR assay. (**D**) The mRNA level of FSP1 was upregulated in MFP M1 treated cells. The relative expression of mRNA level of FSP1 in AC16 cells treated with MFP M1 (20 μM) was assessed by real-time quantitative PCR assay.

All quantitative data are presented as mean ± SD from three independent experiments; and P values were calculated with unpaired t test (*, P <0.05; **, P <0.01; ***, P < 0.001; ****, P <0.0001).

**Figure S4. The upregulation of FSP1 mRNA induced by disrupting mitochondria homeostasis is dependent on NRF2.**

(**A-C**) The upregulation of FSP1 mRNA was blocked by ML385 treatment. **(A)** The relative expression of mRNA level of FSP1 of NT AC16 cells and DRP1 KD AC16 cells treated with ML385(10 μM) for 12 h was assessed by real-time quantitative PCR assay. (**B)** The relative expression of FSP1 mRNA in vector control AC16 cells and OPA1 OE AC16 cells treated with ML385(10 μM) for 12 h was assessed by real-time quantitative PCR assay. (**C)** The relative expression of FSP1 mRNA in control MEFs and MFN1 KO MEFs treated with ML385(10 μM) for 12 h was assessed by real-time quantitative PCR assay. (**D-F**) Knockdown of NRF2 suppressed the upregulation of FSP1 mRNA. The relative expression of mRNA level of FSP1 in the indicated AC16 cells were assessed by real-time quantitative PCR assay. (**G)** Western blot analysis of FSP1 expression in DRP1 KD, OPA1 OE, MFN1 KD and control A549 cells.

All quantitative data are presented as mean ± SD from three independent experiments; and P values were calculated with unpaired t test (*, P <0.05; **, P <0.01; ***, P < 0.001; ****, P <0.0001).

**Figure S5. Defects in mitochondrial dynamics homeostasis promotes NRF2 nuclear accumulation in A549 cells**

(**A-D**) Western blot analysis of the nuclear accumulation of NRF2 in DRP1 KD A549 cells (**A**), OPA1 OE A549 cells (**B**), MFN1 KD A549 cells (**C**) and M1 (20 μM) treated for 12 h A549 cells. GAPDH: the biomarker of cytoplasm (CP), H3: the biomarker of nuclei.

**Figure S6. Phosphorylation of NRF2 by AMPK is required for NRF2 nuclear accumulation, FSP1 upregulation, and ferroptosis resistance in mitochondrial dynamics defected cells**

**(**A) Analysis the level of ATP in indicated cells using the ATP, ADP and AMP assay kit coupled with HPLC analysis. **(**B) Western blot analysis of protein level of ETC components (NDUFS1: complex I, SDHA: complex II, UQCRC1: complex III, COXIV: complex IV and ATP5B: complex V) in indicated cells. **(**C) Measurement of total ROS with H2DCFDA dye staining in indicated cells. (D) Measurement of mitochondrial ROS with MitoSOX dye staining in indicated cells. (E) Western blot analysis of stability of wildtype NRF2 and NRF2-S550A mutant as indicated. Vector-GFP were co-transfected with NRF2-myc or NRF2-S550A-myc as quality control. (F) Western blot analysis of NRF2 expression (Input panel), ubiquitination and interaction with KEAP1 of NRF2 (IP panel) in HEK293T cells transfected wildtype NRF2 or NRF2-S550A mutant. 5 μg indicated plasmids were transfected in HEK293T cells and MG132 (10 μM) was treated in transfected HEK293T cells for 6 h before IP assay. (F) Left: Western blot analysis of the protein level of AMPK-$P^{T172}$ and FSP1 in AC16 cells in glucose depleted medium or control for 12 h. Right: Western blot analysis of the nuclear accumulation of NRF2 in AC16 cells in glucose depleted medium or control for 12 h. GAPDH: the biomarker of cytoplasm (CP), H3: the biomarker of nuclei.

All quantitative data are presented as mean ± SD from three independent experiments; and P values were calculated with unpaired t test (*, P <0.05; **, P <0.01; ***, P < 0.001; ****, P <0.0001).

**Figure S7. MFP M1 does not compromise the chemotherapeutic efficacy of doxorubicin**

(A-C) MFP M1 treatment does not attenuate chemotherapeutic efficacy of doxorubicin in the mouse B16 melanoma cancer model. (D-F) MFP M1 treatment does not attenuate chemotherapeutic efficacy of doxorubicin in the human ACHN kidney cancer model.

All quantitative data are presented as mean ± SD from independent experiments; and P values were calculated with unpaired t test (n=6, *, P <0.05; **, P <0.01; ***, P < 0.001; ****, P <0.0001).

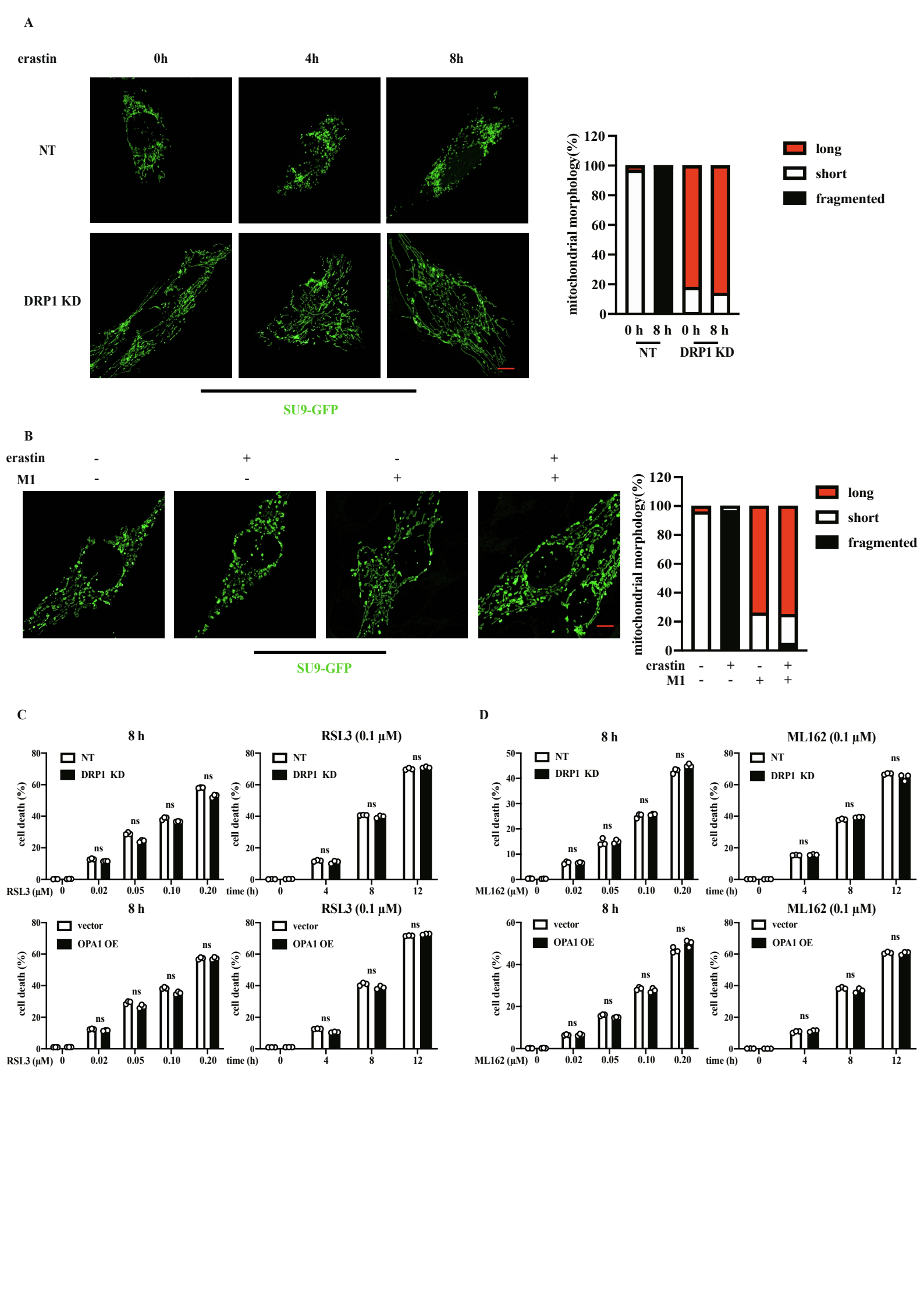
A
erastin
0h
4h
8h
NT
DRP1 KD
SU9-GFP
mitochondrial morphology(%)
120
100
80
60
40
20
0
0 h
8 h
0 h
8 h
NT
DRP1 KD
long
short
fragmented
B
erastin
-
+
-
+
M1
-
-
+
+
SU9-GFP
mitochondrial morphology(%)
120
100
80
60
40
20
0
erastin
-
+
-
+
M1
-
-
+
+
long
short
fragmented
C
8 h
RSL3 (0.1 μM)
NT
DRP1 KD
cell death (%)
RSL3 (μM)
0
0.02
0.05
0.10
0.20
time (h)
0
4
8
12
ns
vector
OPA1 OE
D
8 h
ML162 (0.1 μM)
NT
DRP1 KD
cell death (%)
ML162 (μM)
0
0.02
0.05
0.10
0.20
time (h)
0
4
8
12
ns
vector
OPA1 OE

A

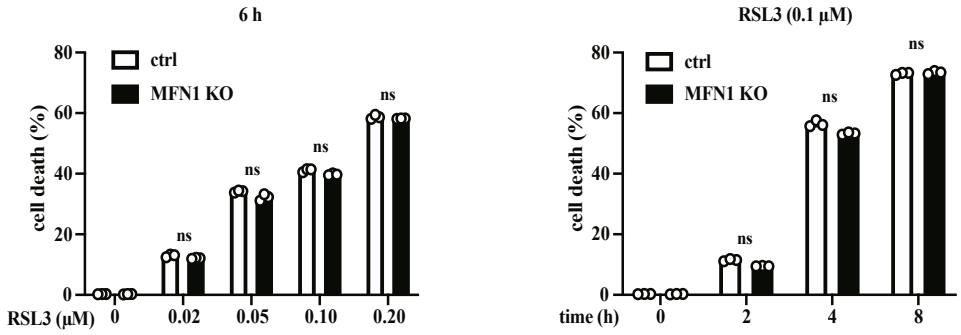
6 h
ctrl
MFN1 KO
cell death (%)
RSL3 (µM)
0
0.02
0.05
0.10
0.20
ns
RSL3 (0.1 µM)
time (h)
0
2
4
8

B

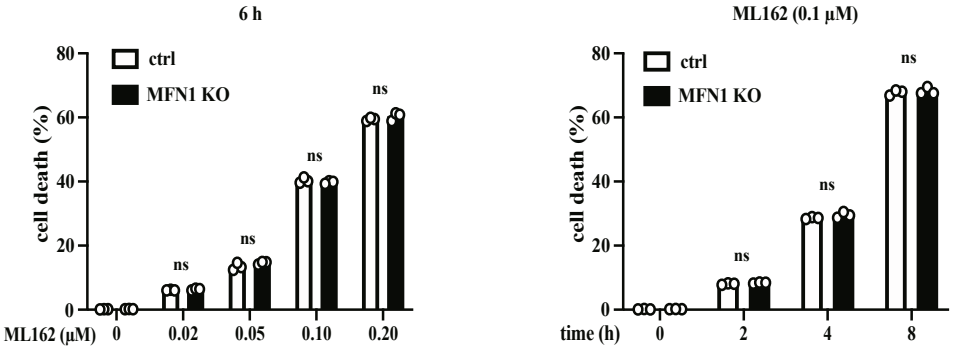
6 h
ctrl
MFN1 KO
cell death (%)
ML162 (µM)
0
0.02
0.05
0.10
0.20
ns
ML162 (0.1 µM)
time (h)
0
2
4
8

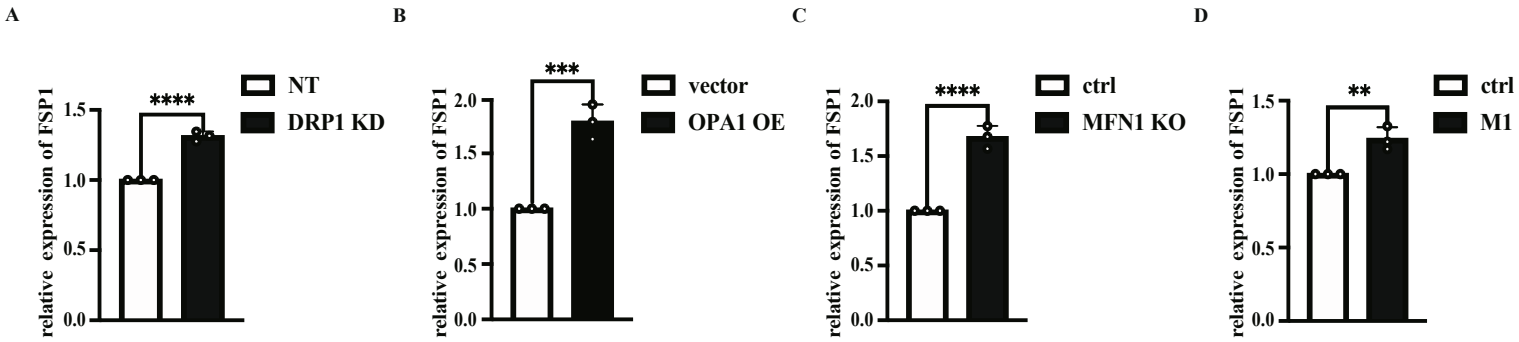
A
B
C
D
relative expression of FSP1
1.5
1.0
0.5
0.0
****
NT
DRP1 KD
2.0
1.5
1.0
0.5
0.0
***
vector
OPA1 OE
2.0
1.5
1.0
0.5
0.0
****
ctrl
MFN1 KO
1.5
1.0
0.5
0.0
**
ctrl
M1

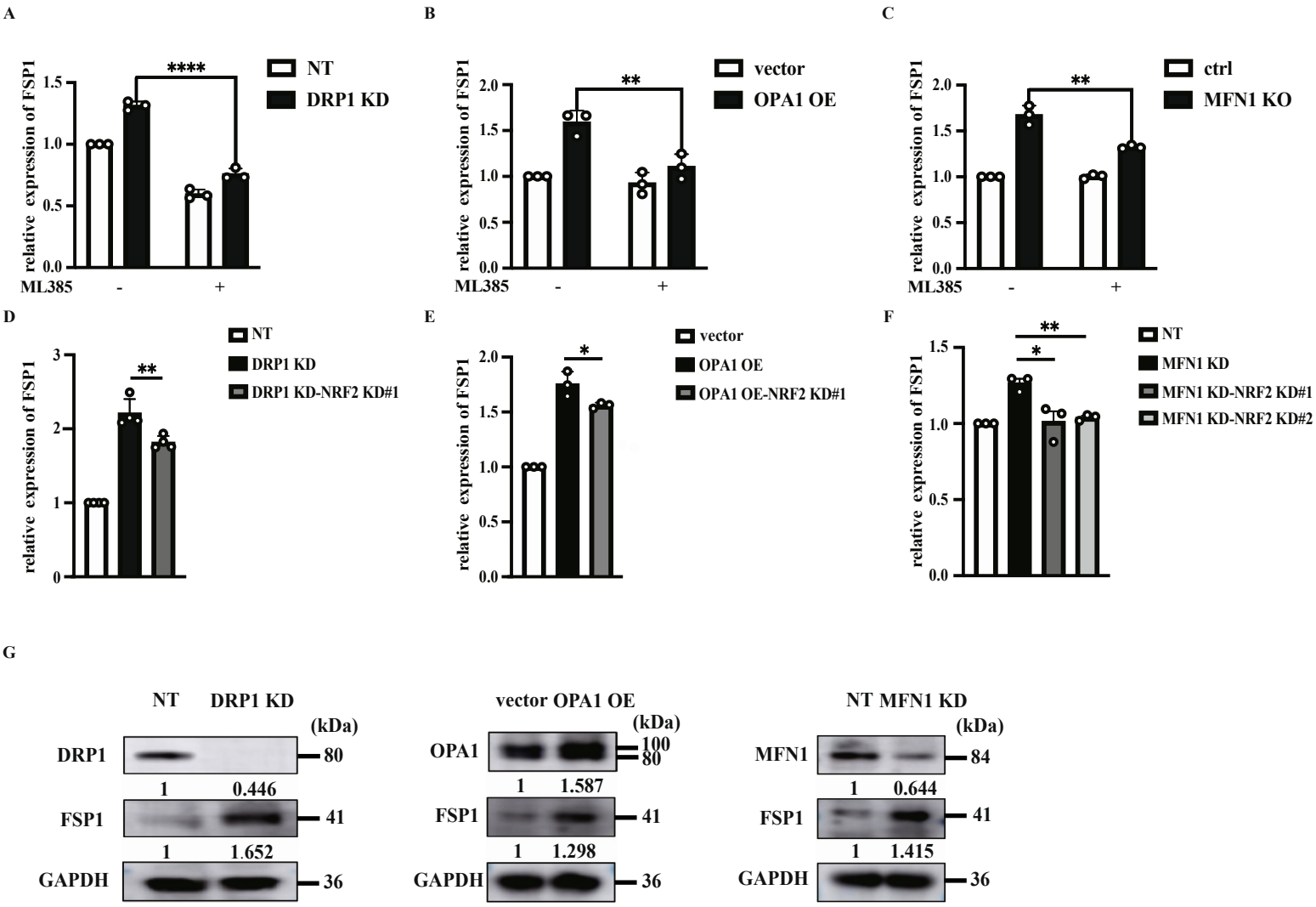
A
relative expression of FSP1
****
NT
DRP1 KD
ML385
-
+
B
relative expression of FSP1
**
vector
OPA1 OE
ML385
-
+
C
relative expression of FSP1
**
ctrl
MFN1 KO
ML385
-
+
D
relative expression of FSP1
**
NT
DRP1 KD
DRP1 KD-NRF2 KD#1
E
relative expression of FSP1
*
vector
OPA1 OE
OPA1 OE-NRF2 KD#1
F
relative expression of FSP1
**
*
NT
MFN1 KD
MFN1 KD-NRF2 KD#1
MFN1 KD-NRF2 KD#2
G
NT
DRP1 KD
(kDa)
DRP1
80
1
0.446
FSP1
41
1
1.652
GAPDH
36
vector OPA1 OE
(kDa)
OPA1
100
80
1
1.587
FSP1
41
1
1.298
GAPDH
36
NT MFN1 KD
(kDa)
MFN1
84
1
0.644
FSP1
41
1
1.415
GAPDH
36

A

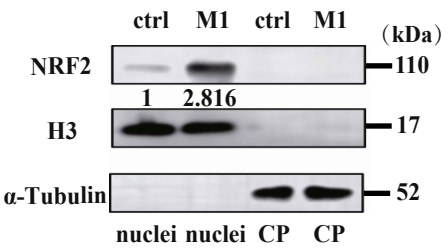
ctrl
M1
ctrl
M1
(kDa)
NRF2
110
1
2.816
H3
17
α-Tubulin
52
nuclei nuclei CP CP

B

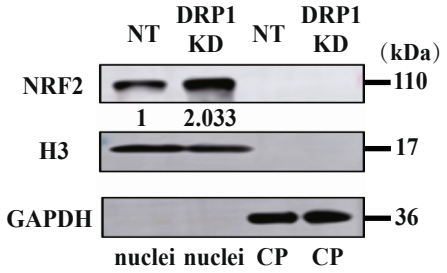
NT
DRP1 KD
NT
DRP1 KD
(kDa)
NRF2
110
1
2.033
H3
17
GAPDH
36
nuclei nuclei CP CP

C

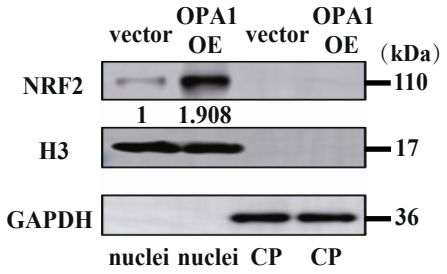
vector
OPA1 OE
vector
OPA1 OE
(kDa)
NRF2
110
1
1.908
H3
17
GAPDH
36
nuclei nuclei CP CP

D

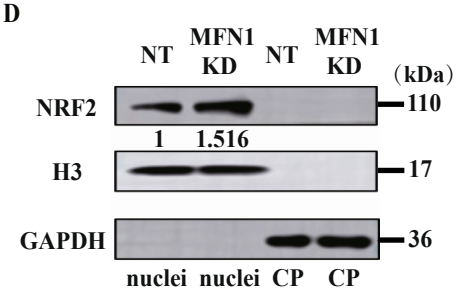
NT
MFN1 KD
NT
MFN1 KD
(kDa)
NRF2
110
1
1.516
H3
17
GAPDH
36
nuclei nuclei CP CP

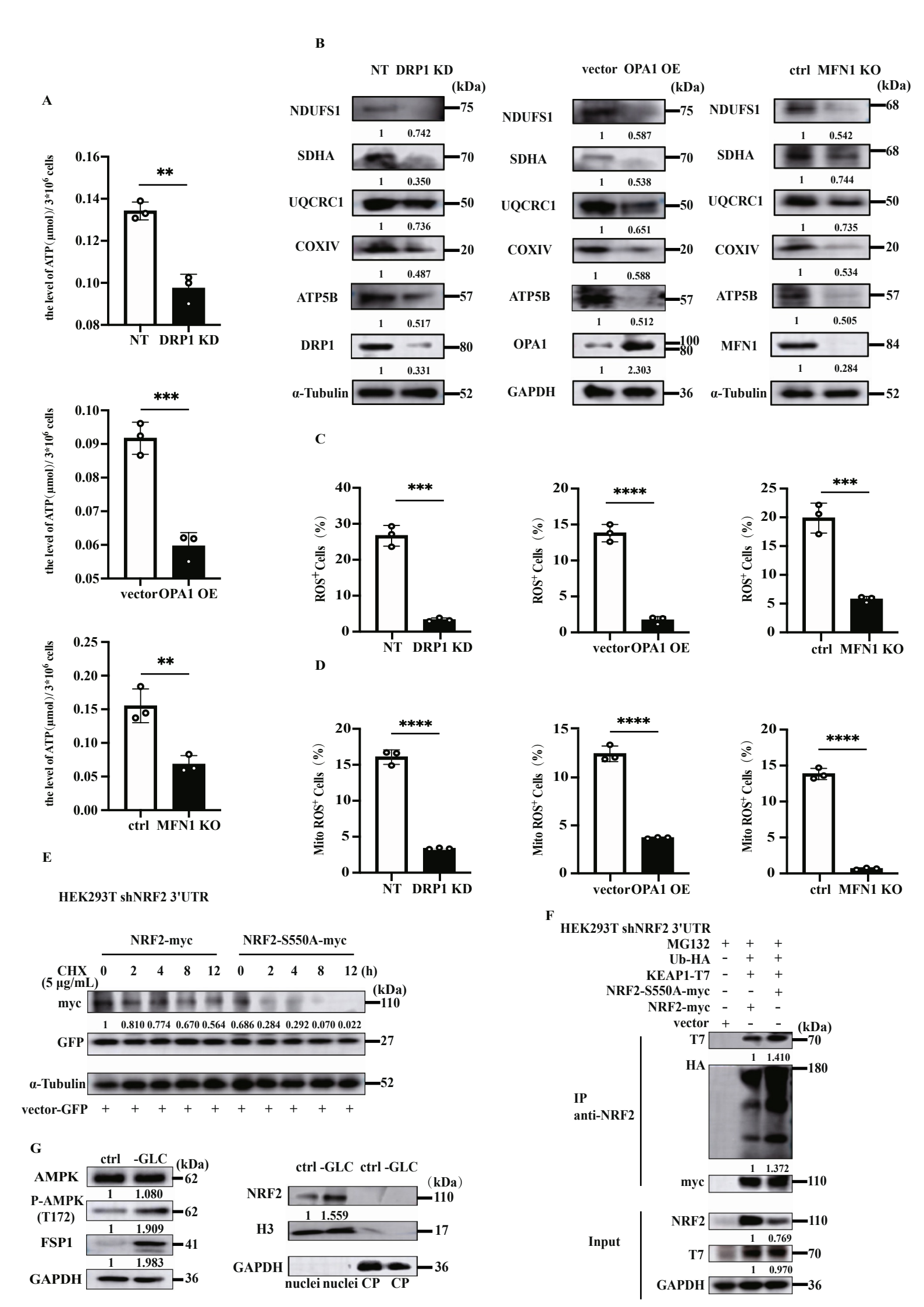
A
B
C
D
E
F
G
the level of ATP (μmol) / 3*10^6 cells
NT DRP1 KD
vector OPA1 OE
ctrl MFN1 KO
NT DRP1 KD (kDa)
vector OPA1 OE (kDa)
ctrl MFN1 KO (kDa)
NDUFS1
SDHA
UQCRC1
COXIV
ATP5B
DRP1
OPA1
MFN1
GAPDH
α-Tubulin
ROS+ Cells (%)
Mito ROS+ Cells (%)
HEK293T shNRF2 3'UTR
NRF2-myc
NRF2-S550A-myc
CHX (5 μg/mL)
0 2 4 8 12 0 2 4 8 12 (h)
myc
GFP
vector-GFP
MG132
Ub-HA
KEAP1-T7
NRF2-S550A-myc
NRF2-myc
vector
T7
HA
IP anti-NRF2
Input
ctrl -GLC
AMPK
P-AMPK (T172)
FSP1
GAPDH
NRF2
H3
nuclei nuclei CP CP

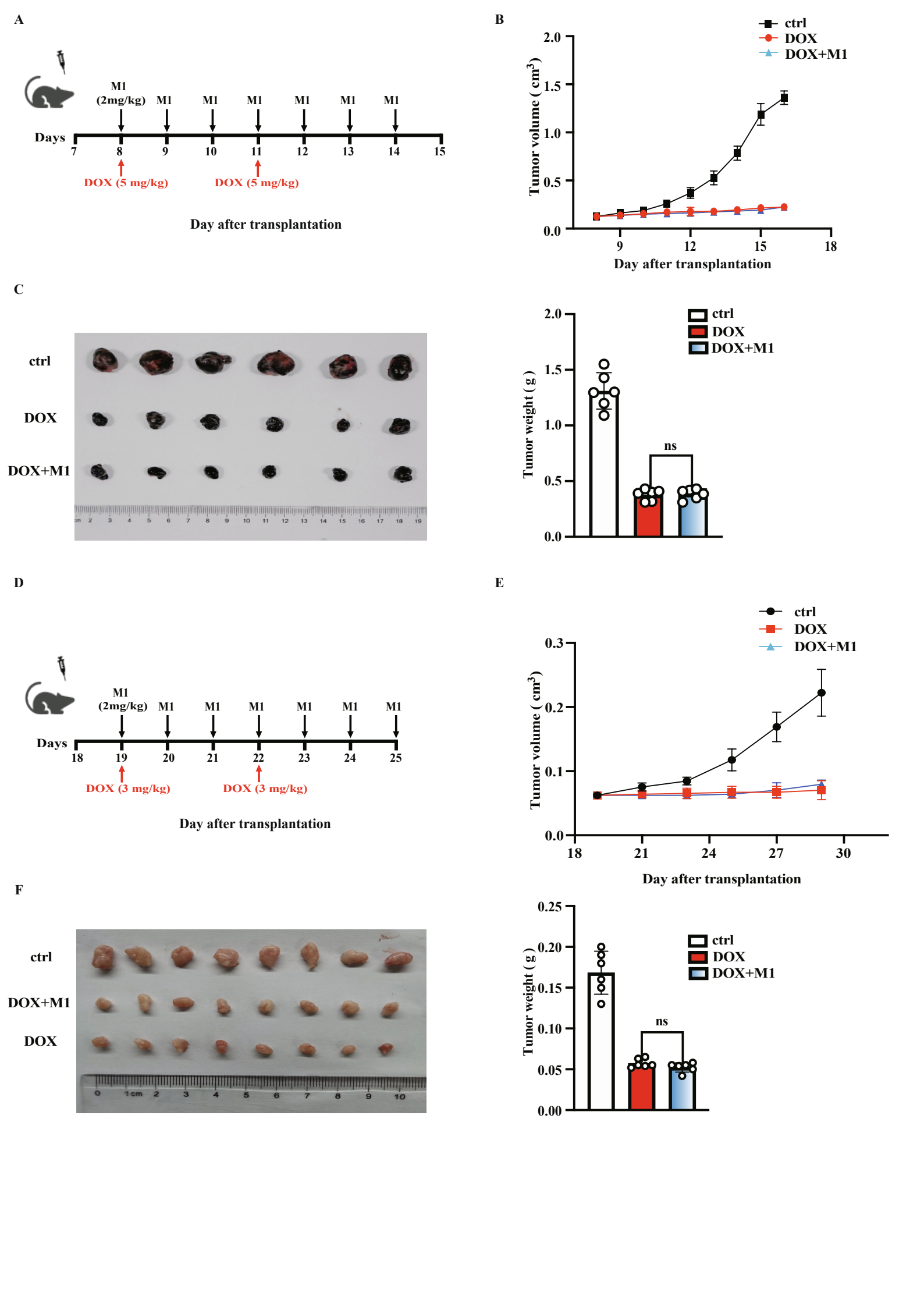
A
M1 (2mg/kg)
M1
M1
M1
M1
M1
M1
Days
7
8
9
10
11
12
13
14
15
DOX (5 mg/kg)
DOX (5 mg/kg)
Day after transplantation
B
ctrl
DOX
DOX+M1
Tumor volume ( cm3)
2.0
1.5
1.0
0.5
0.0
9
12
15
18
Day after transplantation
C
ctrl
DOX
DOX+M1
Tumor weight ( g )
2.0
1.5
1.0
0.5
0.0
ns
D
M1 (2mg/kg)
M1
M1
M1
M1
M1
M1
Days
18
19
20
21
22
23
24
25
DOX (3 mg/kg)
DOX (3 mg/kg)
Day after transplantation
E
ctrl
DOX
DOX+M1
Tumor volume ( cm3)
0.3
0.2
0.1
0.0
18
21
24
27
30
Day after transplantation
F
ctrl
DOX+M1
DOX
Tumor weight ( g )
0.25
0.20
0.15
0.10
0.05
0.00
ns